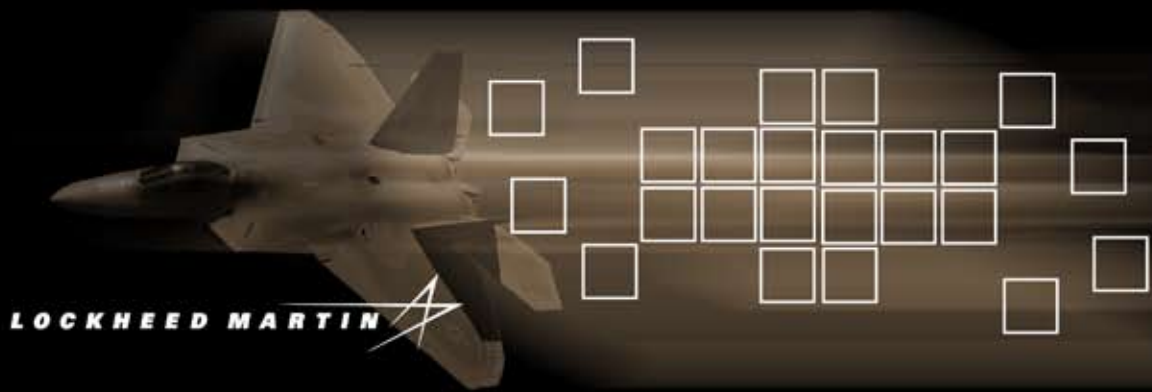
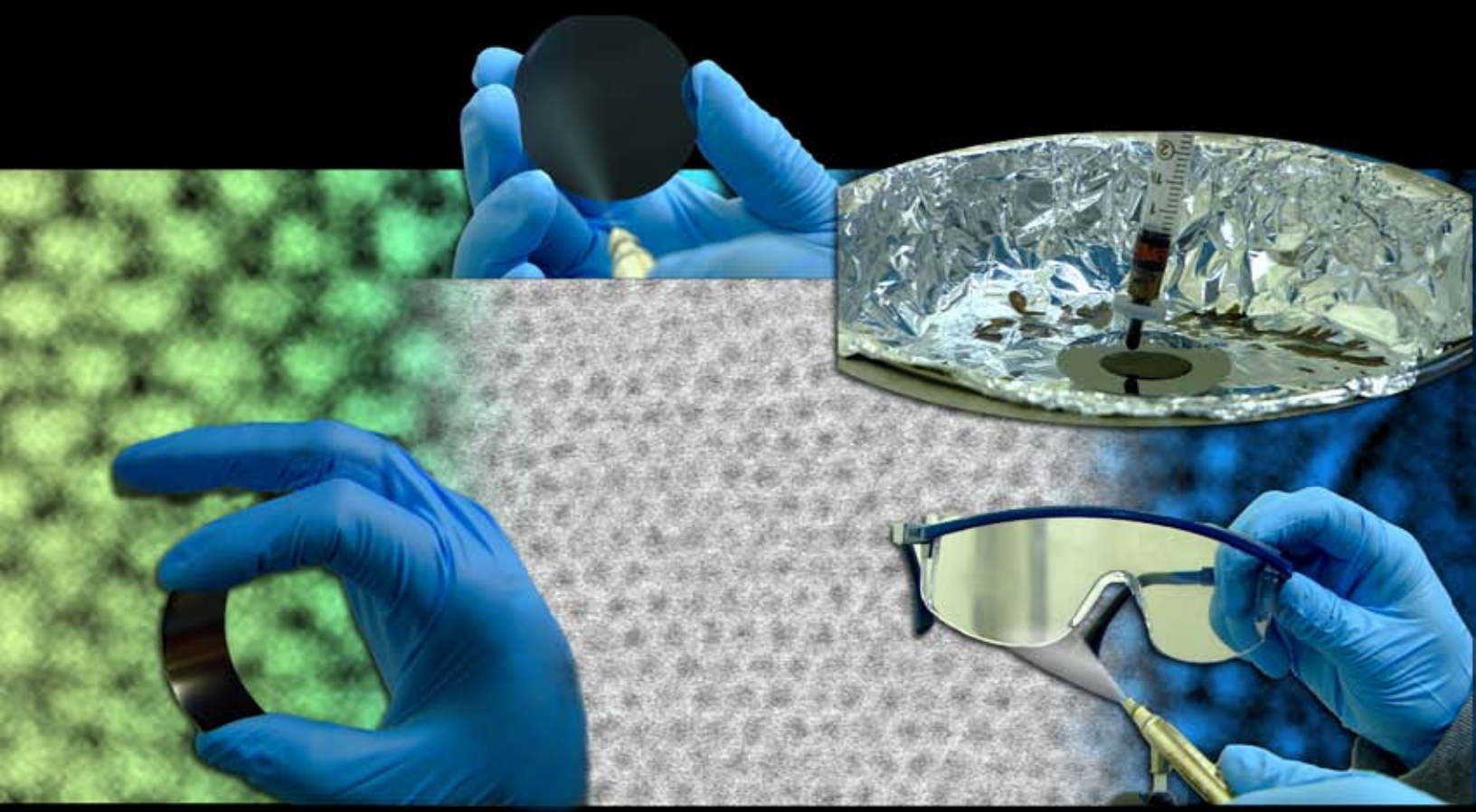


R&D 100 AWARD  ENTRY 2007

SELF-ASSEMBLING PROCESS *for* FABRICATING TAILORED THIN FILMS



LOCKHEED MARTIN 

 Sandia National Laboratories

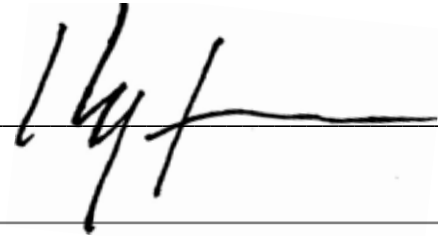
SELF-ASSEMBLING PROCESS *for*
FABRICATING TAILORED THIN FILMS

Submitting Organization

Hongyou Fan
Sandia National Laboratories
Advanced Materials Laboratory
1001 University Boulevard SE
Albuquerque, NM 87106, USA
505-272-7128 (phone)
505-272-7336 (fax)
hfan@sandia.gov

AFFIRMATION: I affirm that all information submitted as a part of, or supplemental to, this entry is a fair and accurate representation of this product.

Submitter's signature _____



Joint Entry

Earl Stromberg
Lockheed Martin Aeronautics
Mail Zone 2893
PO Box 748
Fort Worth, TX 76101, USA
817-763-7376 (phone)
817-762-6911 (fax)
Earl.W.Stromberg@lmco.com

Product Name

Self-Assembling Process for Fabricating Tailored Thin Films

Brief Product Description

This simple, economical nanotechnology coating process enables the development of nanoparticle thin films with architectures and properties unattainable by any other processing method.

Product First Marketed or
Available for Order

August 2006

Inventor or Principal Developer

Hongyou Fan

Member of the Technical Staff at Sandia National Laboratories

Adjunct Professor at the University of New Mexico

Sandia National Laboratories

Advanced Materials Laboratory

1001 University Boulevard SE

Albuquerque, NM 87106, USA

505-272-7128 (phone)

505-272-7336 (fax)

hfan@sandia.gov

Co-Developers

D. Bruce Burckel

Sandia National Laboratories

Ceramic Processing and Inorganic Materials

Advanced Materials Laboratory

1001 University Boulevard SE

Albuquerque, NM 87106, USA

C. Jeffrey Brinker

Sandia National Laboratories

Advanced Materials Laboratory

1001 University Boulevard SE

Albuquerque, NM 87106, USA

Earl Stromberg

Lockheed Martin Aeronautics

Mail Zone 2893

PO Box 748

Fort Worth, Texas 76101, USA

SELF-ASSEMBLING PROCESS *for*
FABRICATING TAILORED THIN FILMS

Product Price

Product price will vary as this new technology is applicable to a wide range of products, from small and irregular shaped parts to large runs of hundreds of square feet of material. Depending on the application-specific performance requirements, the material costs will range from pennies per square foot for simple dielectric films to \$10 per square foot for complex high-performance films.

Patents or Patents Pending

Self-Assembly of Water-Soluble Nanocrystals. Patent application number 10,683,810. (See Appendix A.)

“The broad reach of this rapid self-assembly process, delivering performance across multiple markets, at radically lower cost in an environmentally friendly manner, warrants serious consideration as a top innovation in this decade.”

— Walt Werner, a principal engineer for Lockheed Martin (Maritime Systems and Sensors)

SELF-ASSEMBLING PROCESS *for* FABRICATING TAILORED THIN FILMS

Product's Primary Function

Many of today's technologies and products, including semiconductor devices, consumer electronics, and high-performance optical coatings depend on the ability to produce high-quality thin films. We developed a wet-solution-based process employing self-assembly as a new method to produce optical and electrical thin films. This new process not only meets the demanding requirements of these technologies but also expands the functionality of these films to deliver performance on multiple metrics concurrently. Elegant, simple, and with more options for development and manufacturing than conventional coating processes such as chemical vapor deposition (CVD) or sputtering, our technology involves chemical synthesis of monodisperse nanoparticles with controlled chemical composition, particle size, shape, and their further assembly into engineered nanoparticle composite films.

Tailoring to Specific Product Requirements

Our nanoparticle surface chemistry enables dispersal in readily available commercial solvents, allowing easy and rapid production of films through spin, dip, or spray coating under ambient conditions. During coating, evaporation of solvents induces self-assembly of the nanoparticles to form films of dense, close-packed nanoparticles. In a further refinement, our process is also capable of producing nanocomposite films that are impossible to manufacture through any conventional means. With the addition of secondary organic (e.g., polymers) or inorganic (e.g., silica) components, the nanoparticles self-assemble into ordered arrays embedded in a matrix of the secondary component. The result is an ordered, high-density nanocomposite where the constituent materials are controllably incorporated on the nanometer scale. The functionality of the film can be tailored to a specific product requirement through choice of composition of the nanoparticles, the surrounding framework, or both. The chemical and physical nature of the nanoparticle films (or nanocomposite films) can be further modified (tuned) through a variety of near-ambient processes to tailor unique functions/properties. The ability to adjust material parameters

Product's Primary Function

"The multifunctional ambient deposition of optical coatings eliminates the need for long cycle times and expensive ... capital equipment while providing low stress deposits with improved yields. This technology will greatly improve many of our current and future products. The nanocrystal films will significantly improve the performance of electro-optical targeting systems while driving down the costs due to the increase in reliability. Additional applications of this technology within the Lockheed Martin Corporation include airframes, hulls, and advanced coatings for lenses and mirrors."

— Andrew Green, Director,
Space Systems Technology,
Lockheed Martin Corporation

SELF-ASSEMBLING PROCESS *for*
FABRICATING TAILORED THIN FILMS

of the film at the particle synthesis, deposition, or post-deposition stages provides a powerful advantage over conventional deposition approaches, making possible highly engineered films to address specific material needs.

What We Can Do That Conventional Processes Cannot Do

- Using readily available chemicals, we can fine-tune film composition by using semiconductor, metallic, and/or magnetic nanoparticles to optimize optical, electrical, and/or magnetic properties. For instance, optimal single-layer anti-reflection coatings require a precise match between the substrate index of refraction and the index of refraction of the surrounding medium, following the formula:

$$n_{film} = \sqrt{n_{substrate} n_{medium}}$$

With our wet-solution-based coating process, it is possible to deposit a film and tune the index by changing nanoparticle composition, nanoparticle concentration, or both to exactly match the required index of refraction, thus yielding an optimal single-layer anti-reflecting coating on optical glasses as well as on high-index substrates, such as germanium windows.

- It is not uncommon for optical components with high-performance optical coatings to reside in compartments without climate control. As an example of the tailorability our coatings offer, we can make the surface of our nanoparticle optical films hydrophobic (water contact angle larger than 120°) to avoid fogging and icing problems that can cause deterioration of optical performance/function in situations where the optical device (e.g., sensor windows, optical sensor/detector, etc.) is used in wet/humid or cold environments.

Product's Primary Function

"...The coating process is simple, flexible, and compatible with current semiconductor fabrication process. The ability to adjust material parameters of the film at the particle synthesis, deposition or post deposition stages with low cost and friendly environment provides a powerful new degree of freedom over conventional deposition approaches...

...the quantum effects of individual nanoparticle and the collective behavior resulting from the coupling from neighboring nanoparticles bring new physical properties that are not available for conventional bulk materials, establishes a potential breakthrough building block for fabrication of large memory flash drives..."

*– Youren Xu, Manager,
New Mexico Materials Lab,
Intel Corporation*

SELF-ASSEMBLING PROCESS *for*
FABRICATING TAILORED THIN FILMS

- Ancillary properties of the product can also be addressed by applying the added flexibility our technique offers. As well as nanoparticle choice, the matrix composition can also be fine-tuned to optimize optical, electrical, and/or magnetic properties. For example choosing a polymer matrix yields a film with increased flexibility, while choosing inorganic matrix material produces films with greater hardness. The film durability can be tuned by choice of polymer or inorganic component and by taking advantage of chemical bonding to the surface rather than just physical adhesion methods.
- Modification of the nanoparticle surface chemistry eliminates surface tension and drying stress, factors that can contribute to cracking and delamination in conventionally produced thin films.
- The wet-solution coating process can produce nanoparticle films under ambient conditions without using specialized, expensive equipment. Film thickness (10s of nanometers to 1 micron) can be easily controlled by nanoparticle concentration and coating process parameters (such as coating speed) and large or complex parts that would not fit in most processing equipment can be coated.
- For the first time, quantum effects of individual nanoparticles and the collective behavior resulting from the coupling from neighboring nanoparticles allow development of new physical properties that are not attainable for conventional bulk materials; for instance, fabrication of the gold nanoparticle/silica nanocomposite (see Figure B-1) in a metal-insulator-metal architecture. Due to a collective charge transport mechanism involving hopping of electrons from one gold nanocrystal to another within the coating, a

Product's Primary Function

SELF-ASSEMBLING PROCESS *for*
FABRICATING TAILORED THIN FILMS

highly nonlinear current voltage behavior known as Coulomb blockade occurs. In this situation, the gold nanoparticle array behaves like a supercapacitor that holds and releases charges, establishing an important basis for fabrication of high-density memory chips.

- In addition to performing in many of the same applications as conventional thin film approaches, our approach opens up new product capabilities. For instance, by using lithographically patterned substrates, we can coat magnetic nanoparticle films into difficult-to-fill, high-aspect-ratio pattern features for applications of high-density hard drives or flash memory chips.
- Our approach is compatible with standard semiconductor manufacturing processes, making insertion into standard product flows simple.

Product's Competitors

Our approach works in ambient conditions. Chemical vapor deposition and sputtering approaches require nonambient process conditions. The following comparison matrix highlights some of the most significant differences between our approach and standard CVD and sputtering approaches.

Comparison Matrix

Feature	Our Process	CVD	Sputtering
1.) Equipment Costs	\$10-50K	\$3-10M	\$3-7M
2.) Material Toxicity	Low	High	Low
3.) Tunable Material Properties	Yes	Limited	Limited
4.) Substrate Heating	Room Temperature	100–1000 °C	100–600 °C
5.) High Vacuum	Ambient Pressure	Sometimes Required	Required
6.) Large/Irregular Parts	Easy	Difficult	Difficult
7.) Surface Chemistry Functionalization	Yes	No	No

Improvements Upon Competitive Products or Technologies

SELF-ASSEMBLING PROCESS *for* FABRICATING TAILORED THIN FILMS

Thin film deposition for semiconductor devices, consumer electronics, and high-performance optical coatings is dominated by methods that require nonambient process conditions, including high-temperature and/or high-vacuum. While progress in physical deposition techniques, such as sputtering and CVD, has allowed thin film deposition techniques to generally keep pace with the performance requirements of typical optical and semiconductor applications, this performance comes at a significant cost, impacting budget, logistics, and environmental, safety, and health areas. These impacts and the advantages of our approach are discussed below.

Equipment Costs

The facility and capital expenditures for high-vacuum and/or gas handling equipment make sputtering and CVD processes necessarily more expensive than ambient temperature/pressure application systems, such as spin, dip, or spray coating. Capital expenditures for a high-tech CVD or sputtering system capable of depositing square meters of coating run from \$3M to \$10M for the equipment alone. Dedicated lab space and facilities costs are not factored into this number. Contrast that with a wet-solution-based approach where the high-tech aspect of the coating has already been pushed to the chemistry of the nanoparticle solution, and only “low-tech” equipment such as sprayers, dip-tanks, rollers, and dryers are required.

Material Toxicity

Gas precursors required for conventional CVD processing can be highly toxic. For example, silane is pyrophoric (ignites spontaneously on exposure to air), and arsine is pyrophoric and rapidly fatal at exposures of 250 ppm. Materials with this level of toxicity require significant resources for handling, safeguards, and disposal. The liquid nature of the coating solutions in our approach simplifies the health risk management aspects dramatically. The precursors are so much less toxic than typical CVD process gases that many of our processes can be performed open to the lab environment or, at most, in a vent hood.

Improvements Upon Competitive Products or Technologies

“Applications of this technology within Lockheed Martin Corporation are many and include advanced coatings for adaptive micro mirrors, airframes, airship hulls, and fighter jet lenses ... It is a very unique and attractive alternative to conventional CVD and sputter deposited optical and electrical films with the added benefits of improved logistics, increased producibility and cost reduction.”

— Sharon Smith, Director,
Advanced Technology,
Lockheed Martin Corporation

SELF-ASSEMBLING PROCESS *for*
FABRICATING TAILORED THIN FILMS

Tunable Material Properties

Our approach allows us to tailor material properties at the synthesis, surface chemistry, deposition, or post-deposition stages. CVD and sputtering approaches have only limited pre-deposition tunability.

Substrate Heating

CVD and sputtering often require that the substrate be heated during deposition. CVD processes frequently use substrate heating to provide activation energy to drive precursor splitting and deposition. The properties of sputter-deposited films are typically greatly improved by heating the substrate during deposition. Low-thermal-budget applications that are now emerging in high-value missions are incompatible with high-temperature/high-vacuum thin film deposition techniques. For example, optical coatings are required on plastics and low-softening-temperature glasses that deform at deposition



Figure 1: A high-vacuum based deposition system

temperatures typical of conventional processes, and thermally driven dopant diffusion destroys shallow electrical junctions, which today are measured in nanometers. Our room-temperature approach obviates substrate heating, making deposition on such materials practical.

Improvements Upon Competitive Products or Technologies

SELF-ASSEMBLING PROCESS *for*
FABRICATING TAILORED THIN FILMS

High Vacuum

High vacuum is required for plasma sputtering source and plasma-enhanced CVD processes. High-vacuum equipment has a large footprint and requires dedicated lab space (see Figure 1), making at-assembly-line implementation difficult, and completely eliminating the possibility of in-the-field use. Our approach does not require vacuum of any kind, making it agile and flexible.

Large/Irregular Parts

It is established engineering wisdom that “nature abhors a vacuum.” Achieving and maintaining high vacuum in chambers large enough to coat square meters of material poses a significant challenge. In addition to the large footprint, coating logistics are complicated by the time it takes to pump the chamber down, which scales with the volume of the chamber. The requirement of a high-vacuum for sputtering or environmental chamber for CVD necessarily limits the size of parts to be coated. Our wet-solution-based approach can be used to coat irregular shaped parts by dip, spray, or laminar flow coating (see Figure 2 next page), and can be used on large parts in a continuous roll-to-roll process to coat flexible sheets of material.

Surface Chemistry Functionalization

We can alter/functionalize the surface chemistry of the nanocrystals composing our films prior to coating. The properties of the thin films deposited by sputter deposition and CVD deposition are necessarily bulk-like in nature, controlled by either the properties of the sputter target (sputtering) or the precursor gases (CVD) and therefore have limited surface functionalization capabilities.

- Our nanoparticle approach permits tailoring and functionalizing materials.
- Our process precursors are comparatively inexpensive, environmentally benign, and readily available.

SELF-ASSEMBLING PROCESS *for* FABRICATING TAILORED THIN FILMS

Improvements Upon Competitive Products or Technologies

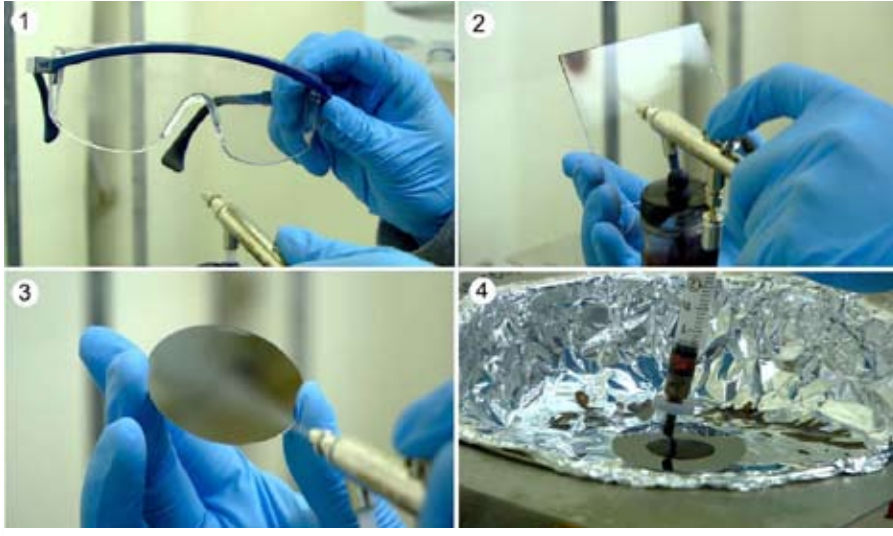


Figure 2. (1) Spray coating anti-reflection layer on a goggle. (2) Spray coating metallic nanoparticle film on a temperature sensitive acrylic. (3) Spray coating magnetic nanoparticle film on a silicon wafer. (4) Spin coating a silicon wafer.

- Lowering the complexity of the deposition equipment allows for thin film deposition to occur in environments that were previously inaccessible, including at the assembly line, or in the field.

- Large and or irregularly shaped parts that cannot fit in available vacuum chambers for CVD or sputtering can be coated with our approach using laminar, spray, or dip coating methods.
- Standard temperature/pressure deposition makes it possible to address low-thermal-budget applications that cannot be serviced using CVD or sputter approaches.

- This technology provides the ability to conduct field repairs, which will improve supportability/logistics and the incorporation of new technology solutions not possible with currently available technology.



LANTIRN sensor assembly on the bottom of an F-16

Principal Applications

“The intent of this effort is to develop this coating technology in order to provide films that possess similar properties to those films that are fabricated with more expensive deposition processes while enabling tailoring of unique functions and properties. In addition, significant applications for industry and the DoD will be identified along with approaches to integrate this technology into our current/future product lines. The resulting tailorable film process and associated applications will have a significant impact on our products (F-16, F-22, F-35, UAVs, etc.).”

— John M. Stratton, Director, New Business Funds and CRADA Management, Advanced Development Programs, Lockheed Martin Aeronautics Company

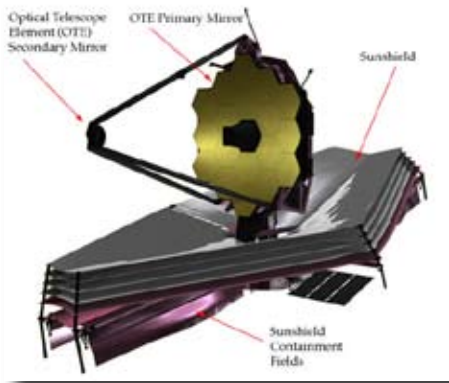
SELF-ASSEMBLING PROCESS *for*
FABRICATING TAILORED THIN FILMS

Sandia National Laboratories partnered with Lockheed Martin Corporation to jointly develop this coating technology; to identify significant applications for industry, the Department of Defense (DoD), Department of Energy (DOE), and National Aeronautics and Space Administration (NASA); and to integrate this technology into product lines. (See CRADA and supporting letters from Lockheed Martin Corporation in Appendices E and F).

The initial application of this technology will be in optical coatings. Products using this technology will have enhanced optical performance, producibility, durability, and supportability. One example of an optical application is as an anti-reflection coating on sensor windows for high-performance military aircraft such as the F-16, F-22, and the F-35 next-generation fighter, as well as UAVs (unmanned air vehicles). The ability to tailor the optical properties of these coatings enhances the optical performance for a wide range of optical sensors, from visual through the infrared. An exciting additional benefit will be supportability. In warfighting operations, these windows are subject to damage from a wide range of environmental factors, especially rain erosion and sand. Window coating repair is expensive and generally requires that the entire unit be removed from the aircraft and shipped to the manufacturer. We expect that this self-assembly technology will allow coatings to be repaired in the field by flight line mechanics, which will significantly reduce both the cost and logistics trail of replacement parts. Lockheed Martin envisions that the sensor system repair kit of the future will include applicator bottles of the coating, much like the touchup paint commonly used today to fix a scratch in car paint.

Another optical application of this technology is for the thermal management of aerostats and high-altitude airships. The application of an infrared-reflective (emissivity control) coating to the exterior of the airbag can be used to improve the stability of the gas inflation pressure across diurnal cycles during

Principal Applications



James Webb Space Telescope



Aerostat Test Balloon

long-term deployment of the lighter-than-air vehicle. This new application method, along with the optical and mechanical properties of this self-assembled thin film coating, is ideally suited to the treatment of the thousands of square feet of flexible fabric required for these large gas-filled structures.

In addition to terrestrial-based applications for optical coatings, there are also space-based applications for this new coating technology. Future extraterrestrial telescopes and earth-sensing satellites will benefit from the flexibility and shock-resistant (both thermal and mechanical) nature of these self-assembled coatings applied to mirrors and optical lenses. The NIRCam (near-infrared camera) for the upcoming James Webb Space Telescope is just such an example where this self-assembly process may provide coatings with improved stability and lower stress over the wide thermal range that the telescope will experience.

Small, thermal-processing-sensitive MEMS (microelectromechanical systems) devices for both terrestrial- and space-based devices, including sensors, will also benefit from the ability of this new coating technology to perform at ambient temperatures. Several device-specific components, such as adaptive micromirrors, which are extremely difficult to coat using conventional thin film coating techniques, have already been identified as excellent candidates for this new coating technology.

All Other Applications



The Desert Hawk, the Air Force's new aid in base protection.

Applications that demonstrate the diverse impact this approach represents include:

1) High-density storage for high-density flash memory:

The ability to manufacture a film with isolated metallic nanoparticles in a dielectric backbone architecture is a building block for high-density memory where the individual components are metallic nanoparticles approximately 2-10 nm in ordered 3D arrays with precisely controlled interparticle spacing of 1-6 nm.

2) High-density 3D interconnects for next-generation electronics:

Placing metallic nanoparticles in a low-viscosity solvent enables filling, and subsequent interconnection, of complex 3D wiring networks, where conduction paths exist without line-of-sight access to the surface.

3) Electrical interconnects for frequency-dependent conductivity:

For some applications, it is desirable to have interconnects with different conductivity, depending on the frequency band. For example, the mechanisms for DC conductivity and RF conductivity are necessarily different. By optimizing material choice and interparticle spacing, we can affect the electron hopping and hence RF conductivity.

4) Magnetic coatings for information storage:

Using our approach, we can deposit metallic nanoparticles into high-density, patterned features to generate the starting material for high-density information storage.

All Other Applications

5) Sensor coatings for chemical and biological sensor platforms:

Nanoparticles of noble metals such as gold and silver are key components to surface-enhanced Raman scattering-based detection methods for chemical and biological sensors. Being able to place the nanoparticles in a rugged, accessible framework with nanometer-level separation increases both the reliability and sensitivity of such sensors.

6) Emissivity-tailored windows:

Controlling the amount of radiant energy reflected/transmitted by windows can help reduce structural heating and cooling loads.

7) Fire shielding:

Materials with high reflectivity in the infrared can be important tools in suppressing the spread of fires within a structure.

SELF-ASSEMBLING PROCESS *for*
FABRICATING TAILORED THIN FILMS

Summary

This process is expected to create a new paradigm for the production of thin films. It will result in significant advantages of reduced costs and increased manufacturing freedom in the production of semiconductor devices, consumer electronics, and high-performance optical coatings. The chemicals and process itself are also environmentally benign. Furthermore, the added flexibility and control over thin film properties open the door for engineered thin films with multiple functions. We feel that the breakthrough we have achieved and its certain impact on thin film deposition make our wet-solution-based self-assembly coating process worthy of consideration for a 2007 R&D 100 Award.

The significance of our achievement is recognized by the scientific community. This technology was published in *Science* and was featured on the covers of *Advanced Functional Materials*, *Chemistry of Materials*, and *Chemical Communications*. (See Appendices C and D.)

Contact Person For Arrangements

Robert W. Carling

Director

Sandia National Laboratories

PO Box 969

Mail Stop 9405

Livermore, CA 94551-0969, USA

925-294-2206 (phone)

925-294-3403 (fax)

rwcarli@sandia.gov

Appendix A

Patents

Appendix B

Images of Films

Appendix C

Science article first disclosing self-assembly coating process, April 23, 2004

Appendix D

Featured scientific journal publications/cover articles

Appendix E

Excerpts of Cooperative Research and Development Agreement

Appendix F

Letters of Support



Appendix A: Patents

This PTO/SB/05 (03-01)

Approved for use through 10/31/2002. OMB 0651-003

U.S. Patent and Trademark Office: U.S. DEPARTMENT OF COMMERCE

Under the Paperwork Reduction Act of 1995, no persons are required to respond to a collection of information unless it displays a valid OMB control number.

19270 U.S. PTO 107683810 100903

UTILITY PATENT APPLICATION TRANSMITTAL <small>(Only for new nonprovisional applications under 37 CFR 1.53(b))</small>		Attorney Docket No. SD7514/S102261	
		First Inventor Hongyou Fan	
		Title Self-Assembly of Water-Soluble Nanocrystals	
		Express Mail Label No. EV332388179US	

APPLICATION ELEMENTS <small>See MPEP chapter 600 concerning utility patent application contents.</small>	ADDRESS TO: Assistant Commissioner for Patents Box Patent Application Washington, DC 20231
--	---

1. <input checked="" type="checkbox"/> Fee Transmittal Form (e.g., PTO/SB/17) <small>(Submit an original and a duplicate for fee processing.) See 37 CFR 1.27.</small> 2. <input type="checkbox"/> Applicant claims small entity status. 3. <input checked="" type="checkbox"/> Specification [Total Pages <input]<br="" type="text" value="19"/> <small>(preferred arrangement set forth below)</small> - Descriptive title of the invention - Cross Reference to Related Applications - Statement Regarding Fed sponsored R & D - Reference to sequence listing, a table, or a computer program listing appendix - Background of the Invention - Brief Summary of the invention - Brief Description of the Drawings (if filed) - Detailed Description - Claim(s) - Abstract of the Disclosure 4. <input checked="" type="checkbox"/> Drawing(s) (35 U.S.C. 113) [Total Sheets <input]<br="" type="text" value="5"/> 5. Oath or Declaration [Total Pages <input]<br="" type="text" value="3"/> a. <input checked="" type="checkbox"/> Newly executed (original or copy) b. <input type="checkbox"/> Copy from a prior application (37 CFR 1.63 (d)) (for continuation/divisional with Box 18 completed) i. <input type="checkbox"/> DELETION OF INVENTOR(S) Signed statement attached deleting inventor(s) named in the prior application, see 37 CFR 1.63(d)(2) and 1.33(b). 6. <input type="checkbox"/> Application Data Sheet. See 37 CFR 1.76	7. <input type="checkbox"/> CD-ROM or CD-R in duplicate, large table or Computer Program (Appendix) 8. Nucleotide and/or Amino Acid Sequence Submission (if applicable, all necessary) a. <input type="checkbox"/> Computer Readable Form (CRF) b. Specification Sequence Listing on: i. <input type="checkbox"/> CD-ROM or CD-R (2 copies); or ii. <input type="checkbox"/> paper c. <input type="checkbox"/> Statements verifying identity of above copies
--	--

ACCOMPANYING APPLICATION PARTS
9. <input type="checkbox"/> Assignment Papers (cover sheet & document(s)) 10. <input type="checkbox"/> 37 CFR 3.753(b) Statement (when there is an assignee) <input type="checkbox"/> Power of Attorney 11. <input type="checkbox"/> English Translation Document (if applicable) 12. <input checked="" type="checkbox"/> Information Disclosure Statement (IDS)/PTO-1449 <input checked="" type="checkbox"/> Copies of IDS Citations 13. <input type="checkbox"/> Preliminary Amendment 14. <input checked="" type="checkbox"/> Return Receipt Postcard (MPEP 503) (Should be specifically itemized) 15. <input type="checkbox"/> Certified Copy of Priority Document(s) (if foreign priority is claimed) 16. <input checked="" type="checkbox"/> Nonpublication Request under 35 U.S.C. 122 (b)(2)(B)(i). Applicant must attach form PTO/SB/35 or its equivalent. 17. <input type="checkbox"/> Other:

18. If a CONTINUING APPLICATION, check appropriate box, and supply the requisite information below and in a preliminary amendment. or in an Application Data Sheet under 37 CFR 1.76:

Continuation Divisional Continuation-in-part (CIP) of prior application _____ / _____

Prior application information: Examiner: _____ Group Art Unit: _____

For CONTINUATION OR DIVISIONAL APPS only: The entire disclosure of the prior application, from which an oath or declaration is supplied under Box 5b, is considered a part of the disclosure of the accompanying continuation or divisional application and is hereby incorporated by reference. The incorporation can only be relied upon when a portion has been inadvertently omitted from the submitted application parts.

19. CORRESPONDENCE ADDRESS

<input checked="" type="checkbox"/> Customer Number or Bar Code Label		<input type="checkbox"/> Correspondence address below
---	--	---

Name		Sandia National Laboratories	
		Intellectual Property Center	
Address		P.O. Box 5800, Mail Stop 0161	
City	Albuquerque, NM 87185	Phone:	(505) 845-8628
		FAX:	(505) 844-2363
Country			

Name (Print/Type)	Elmer A. Klavetter, Registration No. 42,743	
Signature		Date: 10-8-03

Appendix B: Images of Films

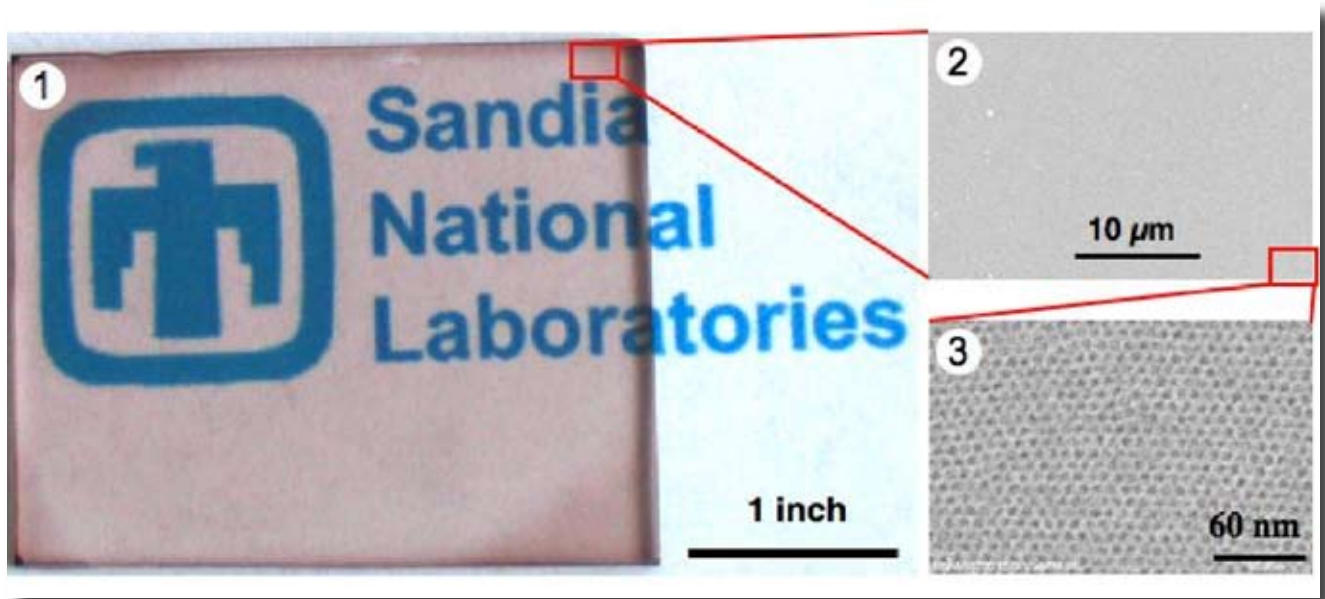


Figure B-1. Photograph of a transparent, self-assembled gold nanoparticle film coated on a microscope slide that covers a Sandia logo. The purple color of the film is indicative of the nanoparticle size.

- (1) Photograph of self-assembled gold nanoparticle film showing uniformity and transparency.
- (2) Scanning electron microscope image of film showing uniformity on the micrometer length scales.
- (3) Transmission electron microscope image showing a uniform hexagonal arrangement of gold nanoparticles within an amorphous silica matrix.

The film was produced by a simple, wet-solution-based, self-assembly coating process at ambient conditions. The ordered nanocrystal assembly is unattainable by alternative chemical or physical deposition processes like CVD or sputtering. This ordered arrangement imparts to the films collective, often nonlinear physical properties due to the properties of the individual nanoparticles and their coupled interactions. Resultant functionality is distinct from that of bulk materials or conventional composites.

Appendix B: Images of Films

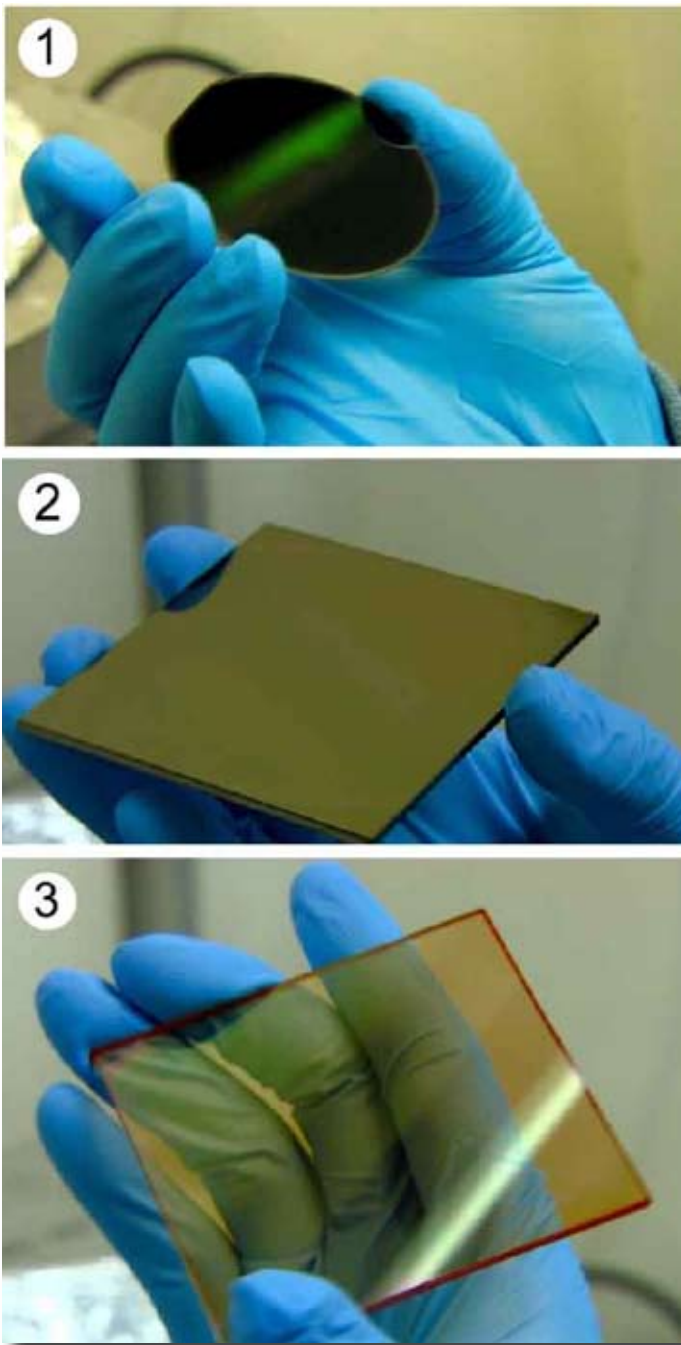


Figure B-2. Examples of various nanoparticle thin films. (1) A gold nanoparticle film on 2×2 silicon wafer. (2) A magnetic nanoparticle film on acrylic plate. (3) A semiconductor nanoparticle film on acrylic plate.

Figure B-2: Examples of various coatings.

Appendix B: Images of Films

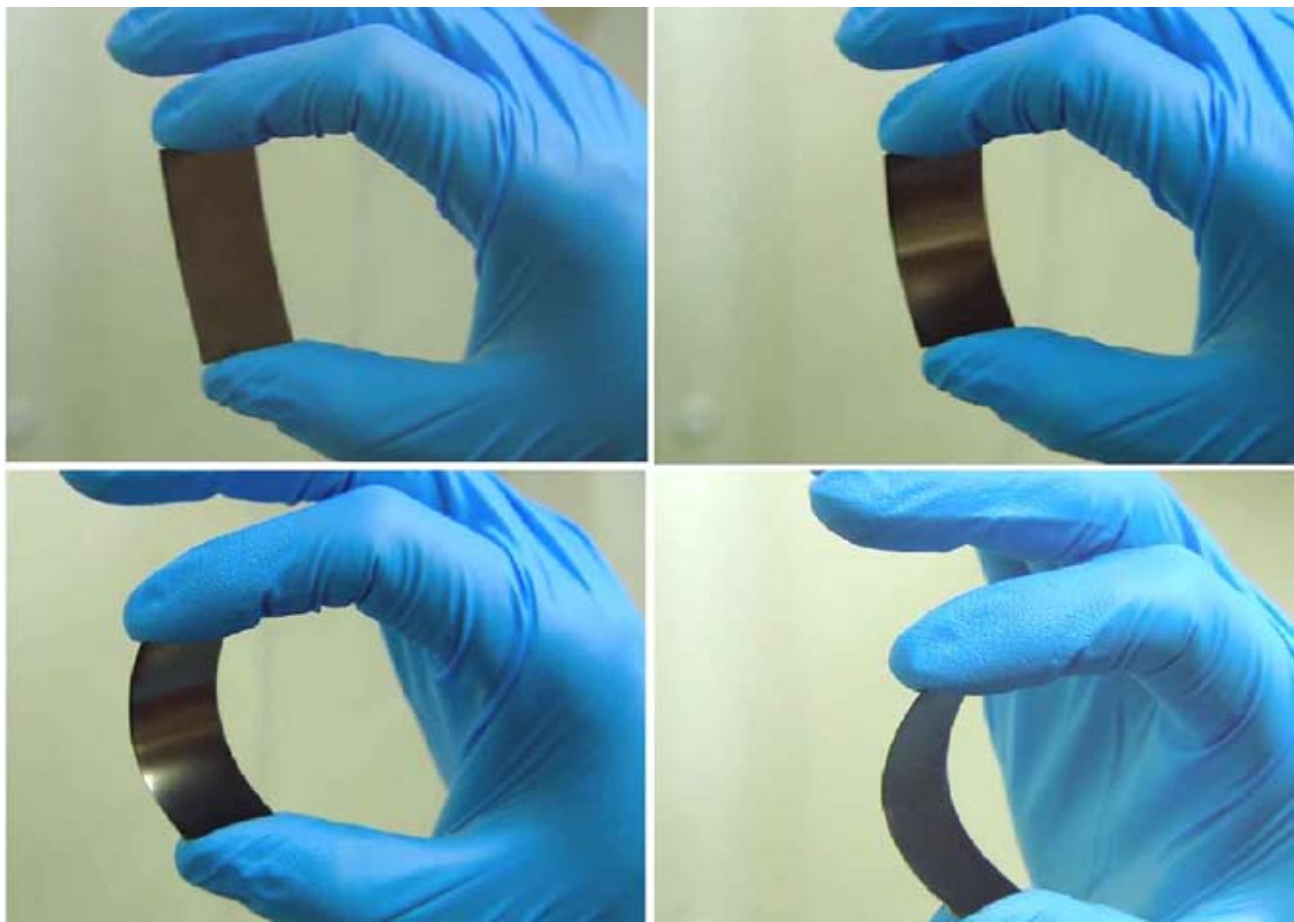


Figure B-3: Nanoparticle film on a temperature sensitive flexible plastic substrate. Coating maintains its mirror finish without cracking.

Figure B-3 contains optical images of a gold nanoparticle film on a temperature-sensitive plastic substrate. This coating was deposited at room temperature to avoid thermal damage to the substrate. Notice that the film maintains its mirror-like quality even after significant bending.

Appendix C: Science article first disclosing self-assembly coating process, April 23, 2004.

SELF-ASSEMBLING PROCESS for FABRICATING TAILORED THIN FILMS

REPORTS

RKKY interaction is not a settled matter (26).

Both single-dot and coupled-dot configurations (27) show roughly linear peak splitting as a function of in-plane magnetic field in the range $B_{\parallel} \sim 2$ to 4 T, with slopes of $\sim 70 \mu\text{eV/T}$. This slope is larger by a factor of ~ 1.5 than expected for the GaAs g factor of 0.44, but is consistent with g -factor measurements in other devices made from the same wafer. Both the single-dot and coupled-dot cases show an unexpected strengthening of the zero-bias peaks with B_{\parallel} before splitting is observed (for $B_{\parallel} < 2$ T). This is not understood at present and will be investigated in more favorable device geometries in future work.

We have demonstrated coherent control of quantum dot spins by a nonlocal RKKY-like interaction. The present results suggest an approach to nonlocal control of spin and entanglement (28–30), which may be relevant to scaling of solid-state quantum information processing beyond the constraint of nearest-neighbor exchange.

References and Notes

1. An introductory review of the Kondo effect in quantum dots is available in L. Kouwenhoven, L. Glazman, *Physics World* **14**, 33 (2001).
2. L. I. Glazman, M. E. Raikh, *JETP Lett.* **47**, 452 (1988).
3. T. K. Ng, P. A. Lee, *Phys. Rev. Lett.* **61**, 1768 (1988).
4. Y. Meir, N. S. Wingreen, P. A. Lee, *Phys. Rev. Lett.* **70**, 2601 (1993).
5. D. Goldhaber-Gordon *et al.*, *Nature* **391**, 156 (1998).
6. A recent review of double quantum dots, with extensive citations to the literature, is available in W. G. van der Wiel *et al.*, *Rev. Mod. Phys.* **75**, 1 (2003).
7. H. Jeong, A. M. Chang, M. R. Melloch, *Science* **293**, 2221 (2001).
8. J. C. Chen, A. M. Chang, M. R. Melloch Matter **1**, cond-mat/0305289 (2003).
9. D. Loss, E. V. Sukhorukov, *Phys. Rev. Lett.* **84**, 1035 (2000).
10. D. Loss, D. P. DiVincenzo, *Phys. Rev. A* **57**, 120 (1998).
11. M. A. Ruderman, C. Kittel, *Phys. Rev.* **96**, 99 (1954).
12. T. Kasuya, *Prog. Theor. Phys.* **16**, 45 (1956).
13. K. Yosida, *Phys. Rev.* **106**, 893 (1957).
14. A. C. Hewson, *The Kondo Problem to Heavy Fermions* (Cambridge Univ. Press, Cambridge, 1993).
15. C. Jayaprakash, H. R. Krishnamurthy, J. W. Wilkins, *Phys. Rev. Lett.* **47**, 737 (1981).
16. B. A. Jones, C. M. Varma, *Phys. Rev. Lett.* **58**, 843 (1987).
17. B. A. Jones, C. M. Varma, *Phys. Rev. B* **40**, 324 (1989).
18. A. Georges, Y. Meir, *Phys. Rev. Lett.* **82**, 3508 (1999).
19. R. Aguado, D. C. Langreth, *Phys. Rev. Lett.* **85**, 1946 (2000).
20. W. Izumida, O. Sakai, *Phys. Rev. B* **62**, 10260 (2000).
21. T. Aono, M. Eto, *Phys. Rev. B* **63**, 125327 (2001).
22. R. Aguado, D. C. Langreth, *Phys. Rev. B* **67**, 245307 (2003).
23. V. N. Golovach, D. Loss, *Europhys. Lett.* **62**, 83 (2003).
24. Y. Utsumi, J. Martinek, P. Bruno, H. Imamura, cond-mat/0310168 (2003).
25. The device was patterned using surface gates (Cr/Au) fabricated by electron-beam lithography. Peripheral dots have a lithographic area of $0.25 \mu\text{m}^2$; the central dot has a lithographic area of $0.35 \mu\text{m}^2$. The device was fabricated on a delta-doped GaAs/AlGaAs heterostructure with electron gas 100 nm below the surface. Mobility $2 \times 10^5 \text{ cm}^2/\text{Vs}$ and two-dimensional electron density $2 \times 10^{11} \text{ cm}^{-2}$ give a transport mean free path of $\sim 200 \mu\text{m}$ in the unpatterned material.
26. C. M. Varma, personal communication.
27. N. J. Craig *et al.*, data not shown.
28. T. J. Osborne, M. A. Nielsen, *Phys. Rev. A* **66**, 032110 (2002).
29. A. Saguia, M. S. Sarandy, *Phys. Rev. A* **67**, 012315 (2003).
30. F. Verstraete, M. Popp, J. I. Cirac, *Phys. Rev. Lett.* **92**, 027901 (2004).
31. We thank C. Varma, B. Halperin, and A. Yacoby for useful discussion. Supported in part by the Defense Advanced Research Projects Agency (DARPA)–Quantum Information Science and Technology (QUIST) program, the Army Research Office under DAAD-19-02-1-0070 and DAAD-19-99-1-0215, and

the NSF–Nanoscale Science and Engineering Center program at Harvard. Research at UCSB was supported in part by iQUIST. Supported by the Harvard College Research Program (N.J.C.), NSF (J.M.T.), and Middlebury College (E.A.L.).

8 January 2004; accepted 11 March 2004

Published online 25 March 2004;

10.1126/science.1095452

Include this information when citing this paper.

Self-Assembly of Ordered, Robust, Three-Dimensional Gold Nanocrystal/Silica Arrays

Hongyou Fan,^{1,2*} Kai Yang,³ Daniel M. Boye,⁴ Thomas Sigmon,³ Kevin J. Malloy,³ Huifang Xu,² Gabriel P. López,² C. Jeffrey Brinker^{1,2*}

We report the synthesis of a new nanocrystal (NC) mesophase through self-assembly of water-soluble NC micelles with soluble silica. The mesophase comprises gold nanocrystals arranged within a silica matrix in a face-centered cubic lattice with cell dimensions that are adjustable through control of the nanocrystal diameter and/or the alkane chain lengths of the primary alkanethiol stabilizing ligands or the surrounding secondary surfactants. Under kinetically controlled silica polymerization conditions, evaporation drives self-assembly of NC micelles into ordered NC/silica thin-film mesophases during spin coating. The intermediate NC micelles are water soluble and of interest for biolabeling. Initial experiments on a metal-insulator-metal capacitor fabricated with an ordered three-dimensional gold nanocrystal/silica array as the “insulator” demonstrated collective Coulomb blockade behavior below 100 kelvin and established the current-voltage scaling relationship for a well-defined three-dimensional array of Coulomb islands.

Despite recent advances in the synthesis and characterization of nanocrystals and NC arrays (1, 2), there remain numerous challenges that limit their practical use. First, for example, synthesis procedures generally used for metallic and semiconducting NCs use organic passivating ligands that make the NCs water insoluble. This is problematic for biological imaging and more generally for uniform incorporation of nanocrystals in hydrophilic matrices like silica or titania needed for the fabrication of robust, functional lasers (3, 4). Second, while steric stabilization of nanocrystals with organic passivating layers suppresses attractive particle-particle interactions, thereby facilitating self-assembly of NC arrays, it necessarily causes the arrays to be mechanically weak and often thermally

and chemically unstable. Third, although evaporation of NC dispersions has been used to prepare quasi-3D NC arrays (5) and films containing isolated 3D NC islands (6), there exist no procedures to reliably fabricate 3D NC arrays as uniform thin films. These combined factors ultimately limit routine integration of nanocrystals into 3D artificial solid devices, in which electronic, magnetic, and optical properties could be tuned through electron charging and quantum confinement of individual NCs mediated by coupling interactions with neighboring NCs (7, 8).

Here, we describe the direct synthesis of water-soluble NC gold micelles and their further self-assembly with silica into robust, ordered 3D NC arrays in bulk or thin-film forms. The synthetic approach is general and avoids the complicated multistep procedures reported previously (9). Our concept is to consider monosized, organically passivated NCs as large hydrophobic molecules that, if incorporated individually into the hydrophobic interiors of surfactant micelles, would result in the formation of monosized NC micelles composed of a metallic (or other) NC core and a hybrid bilayer shell with precisely defined primary and secondary layer thicknesses (Fig. 1H). The hydrophilic NC

¹Sandia National Laboratories, Chemical Synthesis and Nanomaterials Department, Advanced Materials Laboratory, 1001 University Boulevard SE, Albuquerque, NM 87106, USA. ²The University of New Mexico/NSF Center for Micro-Engineered Materials, Department of Chemical and Nuclear Engineering, and ³Center for High Technology Materials, Albuquerque, NM 87131, USA. ⁴Physics Department, Davidson College, Davidson, NC 28035, USA.

*To whom correspondence should be addressed. E-mail: hfan@sandia.gov (H.F.), cjbrink@sandia.gov (C.J.B.)

Appendix C: Science article first disclosing self-assembly coating process, April 23, 2004.

REPORTS

micelle surfaces provide water solubility and allow further assembly or derivatization as depicted in Fig. 1.

To individually incorporate NCs in surfactant micelles, we developed a microemulsion procedure (fig. S1) (10). A concentrated nanocrystal solution, prepared in organic solvent (e.g., chloroform, hexane), is added to an aqueous solution of surfactant with a volume ratio of 1:10 under vigorous stirring to create an oil-in-water microemulsion. Organic solvent evaporation (aided optionally by vacuum or heat treatments) transfers the NCs into the aqueous phase by an interfacial process driven by the hydrophobic van der Waals interactions between the primary alkane of the stabilizing ligand and the secondary alkane of the surfactant, resulting in thermodynamically defined interdigitated bilayer structures (Fig. 1H and fig. S1). For single-tailed

surfactants, an alkane chain of eight or more carbons is required to form micelles with gold nanocrystals stabilized by C_{12} alkanethiols [dodecanethiol (DT)]. Cationic, anionic, and nonionic surfactants, as well as phospholipids, can all form NC micelles (fig. S2), allowing facile control of micelle surface charge and functionality. In addition, fluorescent semiconducting CdSe NCs (stabilized by trioctylphosphine oxide) have been formed into NC micelles with maintenance of optical properties, further supporting the general nature and flexibility of this approach.

The formation and stability of individual gold NC micelles (as opposed to aggregated dimers, trimers, etc.) was confirmed by ultraviolet (UV)-visible spectroscopy and transmission electron microscopy (TEM), where we observed no difference between the positions and widths of the

plasmon resonance bands (~ 510 nm) of the C_{12} -alkanethiol-stabilized gold NCs in chloroform and those of the corresponding water-soluble NC micelles (Fig. 1D). In addition, evaporation of the NC micelle solutions resulted in self-assembly of hexagonally ordered NC arrays (Fig. 1C) as expected for individual, monosized nanocrystals. Judging from UV-visible spectroscopy and TEM and the ability to make ordered arrays, these solutions were stable for more than 2 years at room temperature.

In aqueous media, NC micelles organize hydrophilic components/precursors at the surfactant/water interface through electrostatic and hydrogen-bonding interactions by a mechanism analogous to that of surfactant-directed self-assembly of silica/surfactant mesophases (used as precursors to so-called "mesoporous silicas") (11). For example, addition of tetraethyl orthosilicate (TEOS) under basic conditions produced hydrophilic oligosilicic acid species that organize with NC micelles to form an ordered gold NC/silica mesophase with face-centered cubic (FCC) symmetry (space group Fm3m). Figure 2A, curve b, shows a representative low-angle x-ray diffraction (XRD) pattern of an NC mesophase powder prepared according to pathway i-ii-iii (Fig. 1) by using 2-nm-diameter C_{12} -thiol-stabilized gold NCs, cetyltrimethylammonium bromide (C_{16} TAB) surfactants, and sodium hydroxide catalyst. On the basis of FCC symmetry, the primary peaks are assigned as 111, 220, and 311 reflections. Figure 3, A and B, shows representative TEM images of [001]- and [012]-oriented NC mesophases (prepared as for Fig. 2A, curve b) along with their corresponding electron diffraction patterns. The TEM images are consistent with a unit cell with $a = \sim 10.2$ nm and a uniform, minimum (silica/surfactant) spacing between NCs of ~ 6 nm. This ordered nanocrystal array was formed spontaneously by self-assembly in aqueous media [rather than by solvent evaporation (12)]. Compared with other ordered NC arrays, the embedding silica matrix provides for greater chemical, mechanical, and thermal robustness and, compared with other connected NC systems [for example, those prepared by DNA hybridization (13, 14)], thermodynamically controlled self-assembly provides greater order and control of NC spacing.

Reducing the concentration of the gold NCs, while maintaining a constant surfactant/silica molar ratio, caused the progressive transformation of the cubic, gold NC/silica mesophase to a 2D hexagonal silica/surfactant mesophase (Fig. 2A, curves c and d), as is evident from the greatly diminished (111) reflection in XRD pattern (d) and the appearance of (100), (110), (200), and (210) reflections [Fig. 2A, curve d and magnified inset]. The highly ordered gold NC/silica array

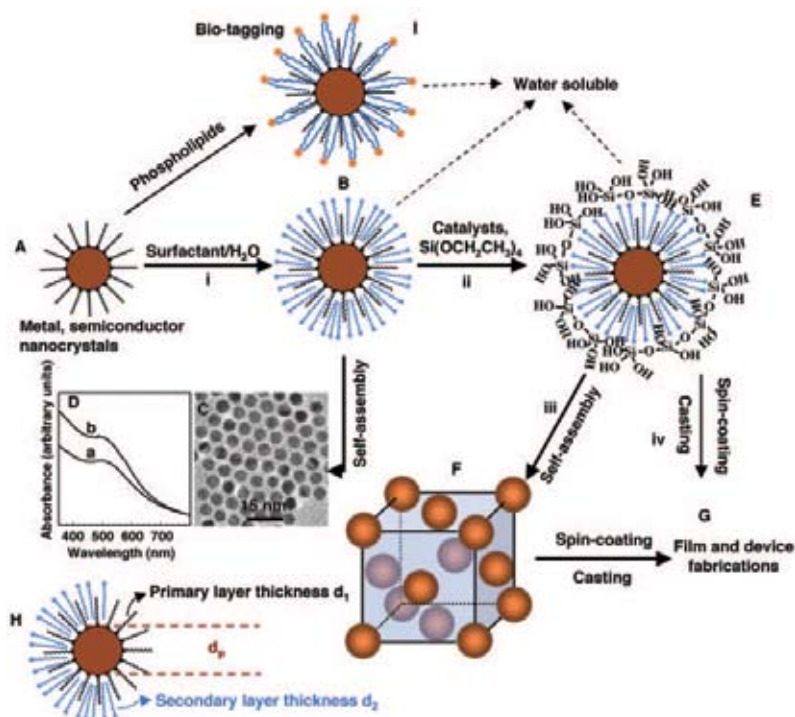


Fig. 1. Processing diagram for the synthesis of water-soluble gold nanocrystal micelles and periodically ordered gold NC/silica mesophases. (A) Gold nanocrystals were prepared according to the method of Brust *et al.* (15), with 1-DT as a stabilizing agent. Heat treatments were employed to further narrow the particle size distributions. (B) Thiol-stabilized nanocrystals are encapsulated in surfactants (using an oil-in-water microemulsion technique) (fig. S1) to form water-soluble NC micelles that, upon evaporation, self-assemble to form hexagonally ordered NC arrays as shown in the TEM image (C). (D) UV-visible spectra of (a) gold nanocrystals in chloroform and (b) gold NC micelles in water; both exhibit plasmon resonance bands at 510 cm^{-1} . (E) Silicic acid moieties formed by hydrolysis of TEOS are organized at the hydrophilic surfactant-water interface of NC micelles, leading, under basic conditions, to a gold NC/silica mesophase (F) composed of NCs organized in a periodic FCC lattice within a dense silica matrix. (G) Under acidic conditions that suppress siloxane condensation, spin coating or casting results in ordered thin-film NC/silica mesophases that are readily integrated into devices. (H) The lattice constant of the NC/silica mesophase is controlled by the nanocrystal size, d_p , the primary layer thickness of the alkanethiol, d_1 , and/or the secondary layer thickness of the surfactant, d_2 (Fig. 2). (I) Polyethylene glycol surfactants or lipids can be used to prepare biocompatible water-soluble NC micelles for biolabeling (27).

REPORTS

forms within a limited NC/surfactant/silica compositional range as expected for a thermodynamically defined mesophase. In this case surfactant and gold are all incorporated into NC micelles, allowing the host framework to be essentially pure, dense silica (polysilicic acid). Highly ordered NC mesophases also require monosized NCs. A broad, poorly defined XRD pattern (Fig. 2A, curve e) was obtained for a gold NC/silica powder sample prepared as in Fig. 2A, curve b, but using gold NCs synthesized according to Brust *et al.* (15) and known to have a rather broad size distribution (~50% compared with ~5% in the present study).

As suggested by Fig. 1H, changing the primary NC particle size d_p , the primary layer thickness d_1 , or the secondary layer thickness d_2 allows adjustment of the NC mesophase lattice constant. For example, Fig. 2B shows the (111) d -spacing to change linearly from ~5.0 to 7.2 nm through variation of d_p from 1.0 to 3.3 nm. Figure 2C shows that changing the secondary layer thickness d_2 by 4 carbon units [$\text{CH}_3(\text{CH}_2)_n(\text{N}(\text{CH}_3)_3^+\text{Br}^-)$, $n_1 = 11$ to $n_m = 15$] results in a 1.11-nm change in (111) d -spacing (1.38 Å/C-C bond), consistent with model predictions and structural studies.

In acidic conditions designed to minimize the siloxane condensation rate (pH ~2), pathway i-ii-iv (Fig. 1) leads to the formation of thin films using standard techniques like spin coating, micromolding, or ink-jet printing. By suppressing siloxane condensation and, thereby, gel formation, solvent evaporation accompanying coating induces self-assembly of NC micelles into NC thin-film mesophases (Fig. 3C) in a manner similar to the evaporation-induced self-assembly of cubic or hexagonal silica/surfactant thin-film mesophases (16). The thin-film XRD pattern (Fig. 2A, curve a) is consistent with a slightly distorted mesophase (face-centered tetragonal) due to constrained 1D shrinkage normal to the substrate surface, observed consistently for thin-film mesophases as a result of siloxane condensation (17). TEM images of films (e.g., Fig. 3C) are qualitatively similar to those of powders, although both XRD and TEM indicate a slightly reduced unit cell dimension ($a \sim 9.6$ nm).

The metallic NC mesophases are highly ordered, fully 3D NC arrays. While several experimental investigations of transport in 1D and 2D ordered arrays have been reported (5, 7, 18), there are no comparable studies performed on high-quality 3D arrays.

As an initial investigation of charge transport, we fabricated planar metal-insulator-metal (MIM) devices, incorporating a Au NC/silica array as the insulator layer (see schematic in Fig. 4), and measured their temperature-dependent current-voltage (I - V) characteristics. Control samples were fabricated by spin coating gold-free silica

sols designed to form silica layers comparable to those of the silica matrices of the NC/silica films.

Samples were mounted on a cold finger, and direct current I - V measurements were performed over the temperature range 300 K to 78 K. The I - V curves for the gold NC/silica capacitors are plotted in Fig. 4A. At room temperature, the I - V curve is linear with a zero-biased resistance of 14 M ohm, corresponding to a film resistivity of about 3×10^6 ohm-cm. Nonlinearity in the I - V behavior near zero bias is evident at 200 K and increases with decreasing temperature. At 100 K and below, conduction occurs through the gold NC/silica insulator only above a minimum threshold voltage, V_T , indicative of a collective Coulomb blockade (19) resulting from electrical isolation of the NCs. Comparison measurements on gold-free control samples showed no noticeable change in the I - V characteristics over this temperature range.

Models of the (low voltage) electron transport in an array of identical Coulomb islands predict a thermally activated behavior of the zero-bias conductance, $G_0 \propto \exp[-E_a/k_B T]$ (20), where E_a is the energy required to charge an electrically neutral nanocrystal and k_B is Boltzmann's constant. The Coulomb charging energy can be expressed as $e^2/2C_0$, where, for a completely isolated NC, the capacitance C_0 depends on the product of the dielectric constant of the surrounding medium ϵ and the nanocrystal radius r , $C_0 = 4\pi\epsilon_0\epsilon r$. Using $r \sim 1.5$ nm for the NC radius (determined by TEM) (Fig. 3A, inset a1) and $\epsilon = 3.9$ for the surrounding silica matrix, C_0 is calculated to be 0.7 aF, corresponding to a Coulomb charging energy of 123 meV.

The temperature-dependent conductance of the Au/silica NC array is presented in Fig. 4A (inset). We observe a strict Arrhenius behavior ($G_0 \propto \exp[-E_a/k_B T]$) over the complete temperature range 78 K to 300 K, attesting to the particle/array uniformity. Two-dimensional NC arrays and granular films in general often show a $G_0 \propto \exp[-(E_a/k_B T)^{1/2}]$ dependence caused by particle-size polydispersity (5, 20, 21). The experimental value of the charging energy, $E_a = 90$ meV, determined from the slope in Fig. 4A (inset), is less than the prediction for an isolated NC.

The temperature-dependent conductance of the Au/silica NC array is presented in Fig. 4A (inset). We observe a strict Arrhenius behavior ($G_0 \propto \exp[-E_a/k_B T]$) over the complete temperature range 78 K to 300 K, attesting to the particle/array uniformity. Two-dimensional NC arrays and granular films in general often show a $G_0 \propto \exp[-(E_a/k_B T)^{1/2}]$ dependence caused by particle-size polydispersity (5, 20, 21). The experimental value of the charging energy, $E_a = 90$ meV, determined from the slope in Fig. 4A (inset), is less than the prediction for an isolated NC.

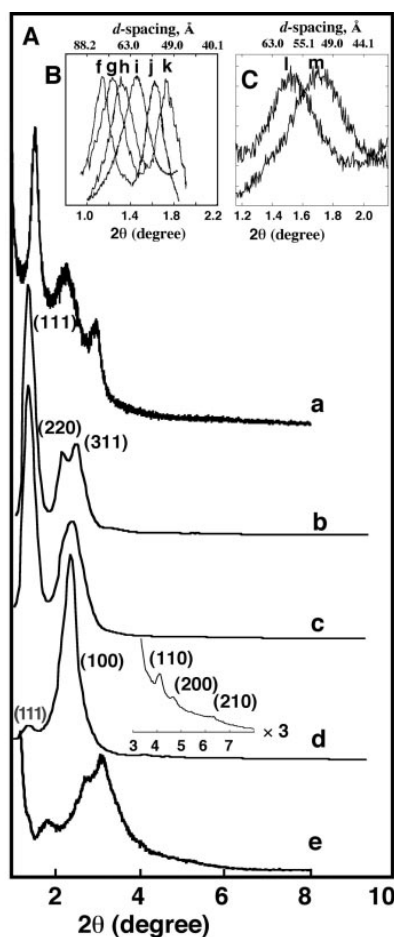


Fig. 2. (A) Representative XRD patterns of gold NC/silica mesophases. (a) Gold NC/silica thin-film mesophase formed by spin coating (Fig. 1, pathway i-ii-iv). The pattern can be indexed as an FCC mesostructure with lattice constant $a = 95.5$ Å. The b, c, and d XRD patterns of bulk gold NC/silica samples were prepared according to pathway i-ii-iii (Fig. 1) by addition of NaOH to an aqueous solution containing TEOS and gold NC micelles. The weight percent of gold NC micelles was progressively reduced from b to d, while the TEOS/surfactant molar ratios were kept constant. (b) Sample was prepared by using 0.36 g 1-DT derivatized gold NCs. The pattern is consistent with an FCC mesostructure with lattice constant $a = 102$ Å. (c) Sample was prepared by using 0.23 g 1-DT derivatized gold NCs. The pattern is similar to that of sample (b). However, the (220) and (311) reflections are not resolved. (d) Sample was prepared by using 0.12 g 1-DT derivatized gold NCs. The XRD pattern (inset magnified $\times 3$) is indexed as a hexagonal silica mesophase with lattice constant $a = 43.4$ Å. A small (111) peak attributable to the NC/silica mesophase is still observed. (e) Sample was prepared by using 0.36 g 1-DT derivatized gold NCs. These NCs were synthesized directly by the method of Brust *et al.* (15) without narrowing the particle size distribution. The amounts of TEOS and surfactant were the same as in b to d. The broader NC size distribution reduces considerably the extent of order. (B) Magnifications of the (111) reflections plotted linearly for samples prepared as in (A)(a), using gold NCs with successively smaller diameters (~33 Å, ~27 Å, ~23 Å, ~17 Å, ~12 Å, ~11 Å). (C) Magnifications of the (111) reflections plotted linearly for samples prepared as in (A)(b), with two different secondary alkane chain lengths of the surfactant [$\text{CH}_3(\text{CH}_2)_n(\text{N}(\text{CH}_3)_3^+\text{Br}^-)$, $n_1 = 15$, $n_m = 11$.

Appendix C: Science article first disclosing self-assembly coating process, April 23, 2004.

REPORTS

Presumably, this discrepancy reflects the reduction of the charging energy arising from the influence of the surrounding nanocrystals. For 2D NC arrays with sufficiently small NC spacings, both modeling and experiment show the charging energy to vary reciprocally with the number of nearest neighbors (5, 7).

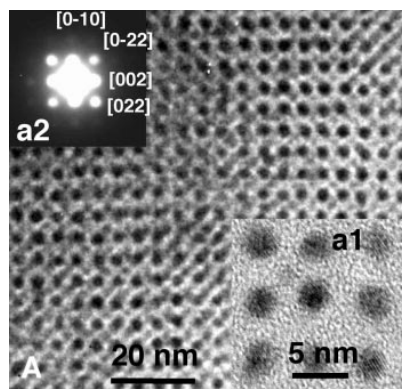
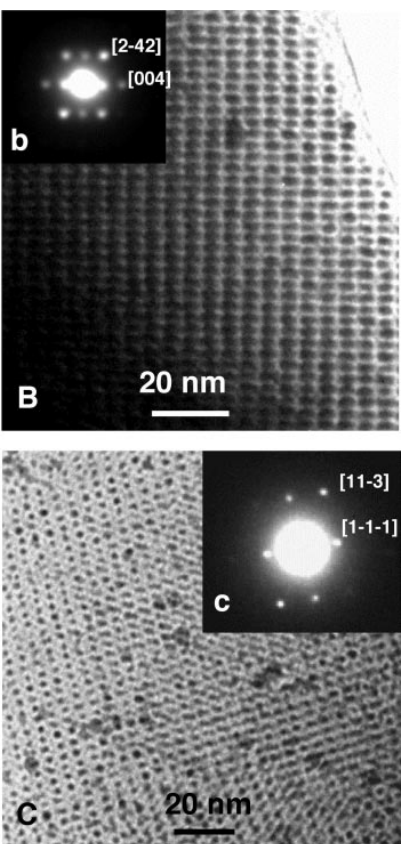


Fig. 3. Representative TEM images of gold nanocrystal/silica mesophases. (A) and (B) [100] and [210] orientations of bulk samples prepared according to pathway i-ii-iii (Fig. 1) and corresponding to Fig. 2A, curve b. (Inset a1) High-resolution TEM of sample (A) showing gold NC lattice fringes. (Inset a2) Selected area diffraction pattern from the image in (A). (Inset b) Selected area electron diffraction from the image in (B). (C) TEM image of [211]-oriented NC/silica thin-film mesophase. (Inset c) Selected area diffraction pattern from image in (C).

Although 3D models of the NC charging energy have not been formulated, it is anticipated that interparticle capacitance could easily account for the 33-meV reduction in E_a observed here.

At low temperatures ($T < 100$ K) where we observe Coulomb blockade behavior, the-



ory predicts that, for $V > V_T$, current scales as a power law, $I = I_0(V/V_T - 1)^\zeta$. The scaling exponent ζ reflects the dimensionality of the accessible current-conducting pathways, and, for 1D and 2D, both modeling (5, 7) and experiment (22) show ζ to equal approximately the array dimensionality. Figure 4B plots representative current-voltage scaling data for our 3D gold/silica NC arrays at 77 K. The results show power-law scaling with $\zeta = 2.7$ (negative bias) and $\zeta = 3.0$ (positive bias). Currently, there are no theoretical predictions or simulations of the 3D scaling exponent; however, the greater value of ζ observed here, compared with previous studies of 2D (22) and quasi-3D arrays (5), is consistent with the greater number of conductive pathways expected for a fully 3D array.

The formation of water-soluble NC micelles and their self-assembly into ordered 3D mesophases provides a new means to integrate model 3D NC arrays into robust devices. The silica host matrix provides compatibility with standard microelectronics processing/patterning and helps eliminate parasitic conductive pathways, enabling higher temperature operation. We expect that by using more surfactant we could provide a mesoporous low k silica host (23), reducing the capacitance and allowing yet higher (i.e., room temperature) operation. The arrays we describe could be the ideal media for the study of the Hubbard Hamiltonian and the variety of transport and collective phenomena predicted to occur for such systems (24, 25). Beyond transport, these robust, highly ordered NC arrays could be useful for catalysts and photonic devices such as lasers (4, 26), and the water-soluble NC micelle intermediates have shown promise for biological labeling or sensors.

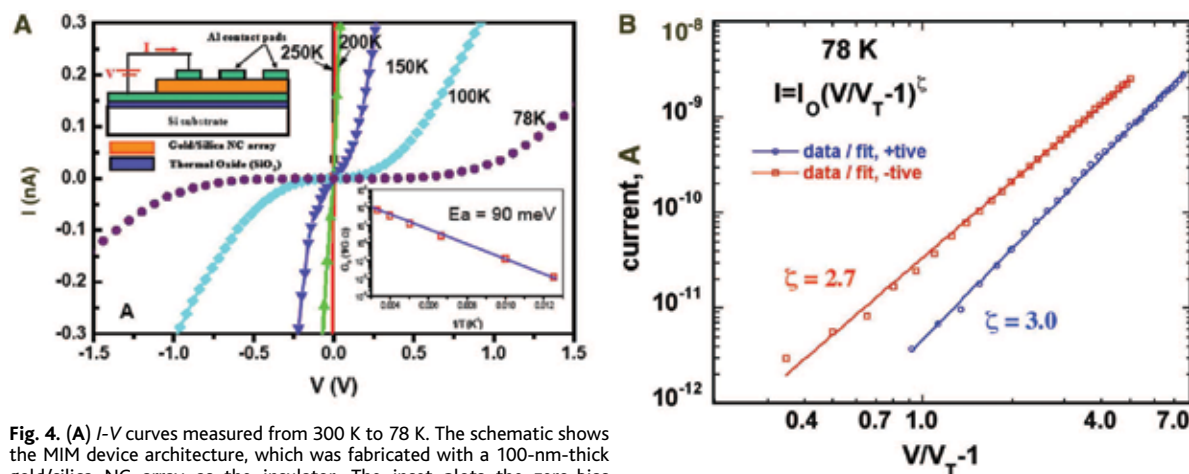


Fig. 4. (A) I - V curves measured from 300 K to 78 K. The schematic shows the MIM device architecture, which was fabricated with a 100-nm-thick gold/silica NC array as the insulator. The inset plots the zero-bias conductance (G_0) versus $1/T$. Data exhibit Arrhenius behavior with activation energy (E_a) of ~ 90 meV. (B) At $T = 78$ K, current displays a power-law dependence for $V > V_T$ with scaling exponent $\zeta = 2.7$ (negative bias) and $\zeta = 3.0$ (positive bias). V_T and ζ were determined by the Levenberg-Marquardt nonlinear least squares method (28) (fig. S3).

Appendix C: Science article first disclosing self-assembly coating process, April 23, 2004.

SELF-ASSEMBLING PROCESS for FABRICATING TAILORED THIN FILMS

REPORTS

References and Notes

- M. A. El-Sayed, *Acc. Chem. Res.* **34**, 257 (2001).
- C. B. Murray, C. R. Kagan, M. G. Bawendi, *Annu. Rev. Mater. Sci.* **30**, 545 (2000).
- V. C. Sundar, H. J. Eisler, M. G. Bawendi, *Adv. Mater.* **14**, 739 (2002).
- M. A. Petruska, A. V. Malko, P. M. Voyles, V. I. Klimov, *Adv. Mater.* **15**, 610 (2003).
- C. T. Black, C. B. Murray, R. L. Sandstrom, S. H. Sun, *Science* **290**, 1131 (2000).
- M. Pileni, *J. Phys. Chem. B* **105**, 3358 (2001).
- A. A. Middleton, N. S. Winggreen, *Phys. Rev. Lett.* **71**, 3198 (1993).
- R. Parthasarathy, C. M. Lin, K. Elteto, T. F. Rosenbaum, H. M. Jaeger, *Phys. Rev. Lett.* **92**, 076801 (2004).
- M. Bruchez, M. Moronne, P. Gin, S. Weiss, A. P. Alivisatos, *Science* **281**, 2013 (1998).
- Details of the synthesis and characterizations are available on Science Online.
- J. Beck et al., *J. Am. Chem. Soc.* **114**, 10834 (1992).
- C. B. Murray, C. R. Kagan, M. G. Bawendi, *Science* **270**, 1335 (1995).
- A. P. Alivisatos et al., *Nature* **382**, 609 (1996).
- C. A. Mirkin, R. L. Letsinger, R. C. Mucic, J. J. Storhoff, *Nature* **382**, 607 (1996).
- M. Brust, M. Walker, D. Bethell, D. J. Schiffrin, R. Whyman, *J. Chem. Soc. Chem. Commun.* **1994**, 801 (1994).
- Y. Lu et al., *Nature* **389**, 364 (1997).
- D. A. Doshi et al., *Science* **290**, 107 (2000).
- C. P. Collier, R. J. Saykally, J. J. Shiang, S. E. Henrichs, J. R. Heath, *Science* **277**, 1978 (1997).
- H. Grabert, M. H. Devoret, *Single Charge Tunneling* (Plenum, New York, 1992).
- C. A. Neugebauer, M. B. Webb, *J. Appl. Phys.* **33**, 74 (1961).
- D. L. Peng, K. Sumiyama, S. Yamamuro, T. Hihara, T. J. Konno, *Appl. Phys. Lett.* **74**, 76 (1999).
- A. J. Rimbberg, T. R. Ho, J. Clarke, *Phys. Rev. Lett.* **74**, 4714 (1995).
- Y. F. Lu et al., *J. Am. Chem. Soc.* **122**, 5258 (2000).
- C. A. Stafford, S. Das Sarma, *Phys. Rev. Lett.* **72**, 3590 (1994).
- G. Kirczenow, *Phys. Rev. B Condens. Matter* **46**, 1439 (1992).
- V. I. Klimov et al., *Science* **290**, 314 (2000).
- B. Dubertret et al., *Science* **298**, 1759 (2002).
- W. H. Press, B. P. Flannery, S. A. Teakolsky, W. T. Vetenling, *Numerical Recipes* (Cambridge Univ. Press, Cambridge, UK, 1986), chap. 14.
- We thank V. Klimov and M. Petruska at Los Alamos National Laboratory for providing CdSe nanocrystals and useful discussions. T. Rieker, NSF (formerly University of New Mexico), performed early XRD experiments. This work was partially supported by the U.S. Department of Energy (DOE) Basic Energy Sciences Program, the Army Research Office, Sandia National Laboratory's Laboratory Directed R&D program and Center for Integrated Nanotechnologies, and the Air Force Office of Scientific Research. TEM investigations were performed in the Department of Earth and Planetary Sciences at the University of New Mexico. Sandia is a multiprogram laboratory operated by Sandia Corporation, a Lockheed Martin Company, for DOE under contract DE-AC04-94ALB5000.

Supporting Online Material

www.sciencemag.org/cgi/content/full/304/5670/567/DC1

Materials and Methods

Figs. S1 to S3

29 December 2003; accepted 17 March 2004

Probabilistic Integrated Assessment of "Dangerous" Climate Change

Michael D. Mastrandrea^{1*} and Stephen H. Schneider²

Climate policy decisions are being made despite layers of uncertainty. Such decisions directly influence the potential for "dangerous anthropogenic interference with the climate system." We mapped a metric for this concept, based on Intergovernmental Panel on Climate Change assessment of climate impacts, onto probability distributions of future climate change produced from uncertainty in key parameters of the coupled social-natural system—climate sensitivity, climate damages, and discount rate. Analysis with a simple integrated assessment model found that, under midrange assumptions, endogenously calculated, optimal climate policy controls can reduce the probability of dangerous anthropogenic interference from ~45% under minimal controls to near zero.

Article 2 of the United Nations Framework Convention on Climate Change (UNFCCC) states its ultimate objective as "Stabilization of greenhouse gas concentrations in the atmosphere at a level that would prevent dangerous anthropogenic interference with the climate system" (1). This level should be achieved within a time frame sufficient to allow ecosystems to adapt naturally to climate change, to ensure that food production is not threatened, and to enable economic development to proceed in a sustainable manner. Thus, the criteria for identifying "dangerous anthropogenic interference" (DAI) may be characterized in terms of the consequences (or impacts) of climate change (2). Although these impacts, and a precise definition of DAI, are subject to considerable uncertainty, a plausible

uncertainty range can be quantified from current scientific knowledge (3). We argue that climate change policy decisions should be conceptualized in terms of preventing or reducing the probability of DAI, a risk-management framework familiar to policymakers and an outcome to which more than 190 signatories to the UNFCCC have committed.

Research related to global climate change must deal explicitly with uncertainty about future climate impacts. Due to the complexity of the climate change issue and its relevance to international policymaking, careful consideration and presentation of uncertainty is important when communicating scientific results (2, 4–7). Policy analysis regarding climate change necessarily requires decision-making under uncertainty (8–10). Without explicit efforts to quantify the likelihood of future events, users of scientific results (including policy-makers) will undoubtedly make their own assumptions about the probability of different outcomes, possibly in ways that the original authors did not intend (11, 12).

Assigning likelihoods to potential future worlds is difficult, as noted by Grüber and Nakicenovic (13), because any such estimates will be highly subjective and based on assessments of future societal behavior and values. Uncertainty, they warn, may alternatively be dismissed or replaced by spurious expert opinion. Although the suitability and effectiveness of techniques for presenting uncertain results is context-dependent, we believe that such probabilistic methods are more valuable for communicating an accurate view of current scientific knowledge to those seeking information for decision-making than assessments that do not attempt to present results in probabilistic frameworks (14).

We present a metric for assessing DAI: a cumulative density function (CDF) of the threshold for dangerous climate change. We demonstrate its utility by applying it to modeled uncertainty in future climate change using an optimizing integrated assessment model (IAM). IAMs are common policy analysis tools that couple submodels of the climate and economic systems, balance costs and benefits of climate change mitigation to determine an "optimal" policy (15), and often exhibit properties not apparent in either submodel alone (16).

We chose Nordhaus' Dynamic Integrated Climate and Economy (DICE) model (17) for our analysis because of its relative simplicity and transparency, despite its limitations (16, 18). The IAM framework allows us to explore the effect of a wide range of mitigation levels on the potential for exceeding a policy-important threshold such as DAI. We do not recommend that our quantitative results be taken literally, but we suggest that our probabilistic framework and methods be taken seriously. They produce general conclusions that are more robust than estimates made with a limited set of scenarios or without probabilistic presentations of outcomes, and our threshold metric for DAI offers a risk-man-

¹Interdisciplinary Graduate Program in Environment and Resources, ²Department of Biological Sciences and Center for Environmental Science and Policy, Stanford University, Stanford, CA 94305, USA.

*To whom correspondence should be addressed. E-mail: mikemas@stanford.edu

Appendix D: Featured scientific journal publications/cover articles.

SELF-ASSEMBLING PROCESS *for*
FABRICATING TAILORED THIN FILMS

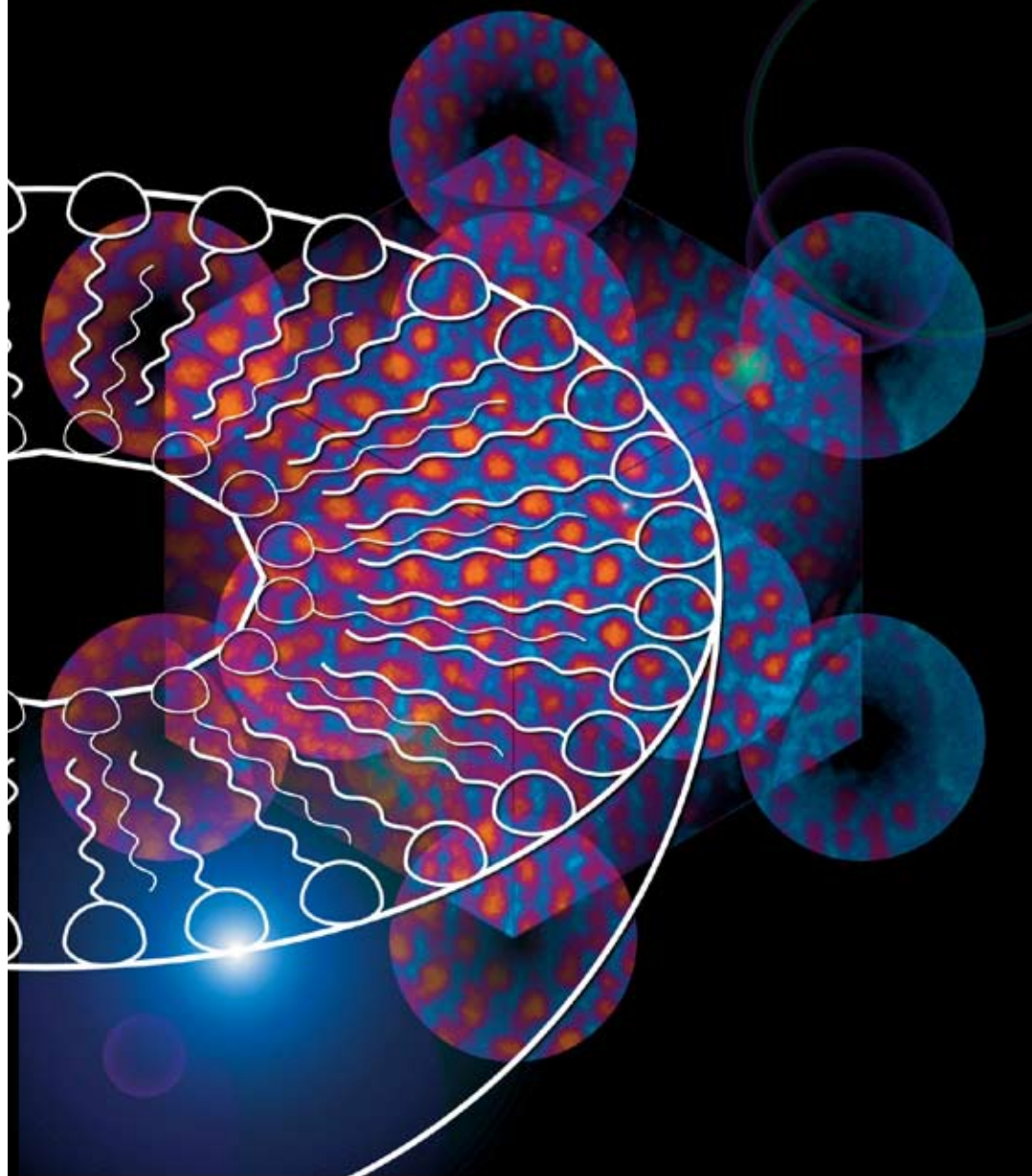
AFMDC6
ISSN 1616-301X
Vol. 16, No. 7
May 2, 2006



WILEY-
VCH

D53313

ADVANCED FUNCTIONAL MATERIALS



3D Ordered Au Nanocrystal/SiO₂ Thin Films

DOI: 10.1002/adfm.200500603

Three-Dimensionally Ordered Gold Nanocrystal/Silica Superlattice Thin Films Synthesized via Sol–Gel Self-Assembly**

By Hongyou Fan,* Adam Wright, John Gabaldon, Adrian Rodriguez, C. Jeffrey Brinker, and Ying-Bing Jiang

Nanocrystals and their ordered arrays hold many important applications in fields such as catalysis, surface-enhanced Raman spectroscopy based sensors, memory storage, and electronic and optical nanodevices. Herein, a simple and general method to synthesize ordered, three-dimensional, transparent gold nanocrystal/silica superlattice thin films by self-assembly of gold nanocrystal micelles with silica or organosilsesquioxane by spin-coating is reported. The self-assembly process is conducted under acidic sol–gel conditions (ca. pH 2), ensuring spin-solution homogeneity and stability and facilitating the formation of ordered and transparent gold nanocrystal/silica films. The monodisperse nanocrystals are organized within inorganic host matrices as a face-centered cubic mesostructure, and characterized by transmission electron spectroscopy and X-ray diffraction.

1. Introduction

Nanocrystals (NCs) exhibit unique size-dependent optical, electronic, and chemical properties. The ability to adjust properties by controlling size, shape, composition, crystallinity, and structure has led to a wide range of potential applications for NCs in areas such as optics, electronics, catalysis, magnetic storage, and biological labeling.^[1–6] Furthermore, NC assembly into 2D and 3D superlattices is of interest for development of “artificial solids” with collective optical and electronic properties that can be further tuned by the NC spacing and arrange-

ment.^[7–11] To date, there have been three approaches to the fabrication of superlattice solids and thin films. The most commonly used approach involves evaporating a drop of NC organic solution on a solid support (e.g., a transmission electron microscopy (TEM) grid, mica, highly ordered pyrolytic graphite (HOPG), etc.), forming face-centered cubic (fcc), body-centered cubic (bcc), or hexagonal close-packed (hcp) superlattice films.^[2,12–14] Heath and co-workers reported a method to form 2D hcp superlattice films of silver NCs by Langmuir–Blodgett deposition.^[9] In a third approach, a homogenous precipitation of superlattice solids was prepared by the slow addition of non-solvents into an NC organic solution.^[15,16] Over a long aging time, well-shaped crystal superlattice solids with fcc structure were finally obtained. The common problem in these approaches is that the NCs that have been used are alkane-chain stabilized, and are therefore hydrophobic and soluble only in organic solvents. The formation of an ordered NC superlattice is limited to organic solvents, and relies on the van der Waals interactions between interdigitated alkane chains surrounding the NCs. The thermally defined, interdigitated alkane chains result in weak mechanical stability of the superlattice. In such materials, charge transport is conducted through the interdigitated organic media between NCs.^[7–11] Recent results indicate that it is desirable to incorporate NCs in inorganic thin film matrices such as silica or titania for achieving chemical and mechanical robustness and enhanced device functionality.^[17–19] Early efforts focused on the encapsulation of metal NCs inside sol–gel matrices by introduction of metal nanoparticles^[20] or metal precursors followed by either thermal decomposition or reduction.^[21,22] Recently, mesoporous materials have been used as templates to create hybrid silica materials infiltrated with metal or semiconducting NCs.^[23–27] There are several disadvantages of the above methods, which include: 1) the NC arrays inside the final materials exhibit a poorly defined or less-ordered structure. This is problematic for fundamental studies of charge transport, where repeatable/reproducible results are required.

[*] Prof. H. Fan, Prof. C. J. Brinker
Chemical Synthesis and Nanomaterials Department
Advanced Materials Laboratory
Sandia National Laboratories
1001 University Blvd. SE, Albuquerque, NM 87106 (USA)
E-mail: hfan@sandia.gov

Prof. H. Fan, A. Wright, J. Gabaldon, A. Rodriguez,
Prof. C. J. Brinker
NSF Center for Micro-Engineered Materials
Department of Chemical and Nuclear Engineering
University of New Mexico
Albuquerque, NM 87131 (USA)
Dr. Y.-B. Jiang
Earth and Planetary Sciences
University of New Mexico
Albuquerque, NM 87131 (USA)

[**] This work was partially supported by the U.S. Department of Energy (DOE) Basic Energy Sciences Program, Sandia National Laboratory's Laboratory Directed R&D program, the Air Force Office of Scientific Research, and Center for Integrated Nanotechnologies (CINT). We acknowledge use of the SEM facility at University of New Mexico supported by the NSF EPSCOR and NNIN grants. TEM investigations were performed in the Department of Earth and Planetary Sciences at the University of New Mexico. Sandia is a multiprogram laboratory operated by Sandia Corporation, a Lockheed Martin Company, for the United States Department of Energy's National Nuclear Security Administration under Contract DE-AC04-94AL85000.

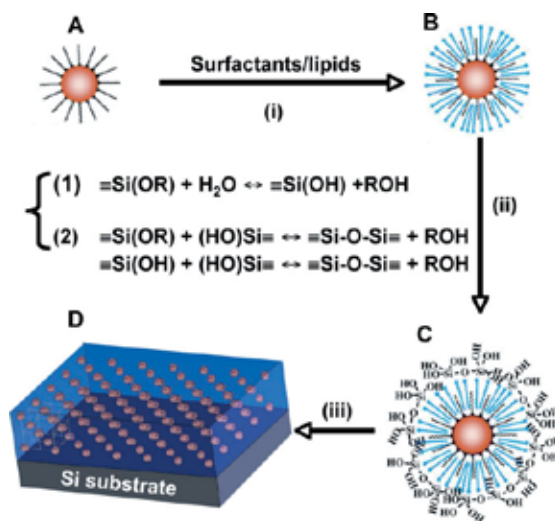
2) The methods have less control over particle sizes and loading. 3) It is difficult to control the interparticle spacing precisely using these methods, and that is essential for achieving new physical properties resulting from coupling between neighboring nanoparticles.^[9,11,28]

We recently reported a facile synthesis of water-soluble NC micelles^[29-31] and their self-assembly into ordered, 3D gold-NC/silica superlattice arrays in a sol-gel process.^[19] Under basic conditions, fast silica hydrolysis and condensation led to a heterogeneous self-assembly system and ordered arrays in solid/powder form.^[19] For device fabrication, thin films are more desirable than powder. Herein, we report a detailed synthesis of gold-NC/silica arrays in thin film form by a slow sol-gel process under acidic conditions. We discovered that silica condensation played an important role in the formation of ordered 3D gold-NC/silica arrays. It is essential that the coating solution be homogeneous to form ordered, transparent gold/silica thin films without cracking. Extensive silica condensation leads to a less-ordered gold/silica mesophase. To this end, the precursor solution was prepared under acidic conditions (ca. pH 2), using the addition of aqueous hydrogen chloride, to maximize the silica gel time and facilitate the self-assembly and formation of ordered NC/silica thin films.^[32,33] By using organosilsesquioxane, we were able to tune the framework chemistry and dielectrics. The final film consists of monodisperse gold NCs arranged within a silica or organosilsesquioxane host matrix in an fcc mesostructure with precisely controlled interparticle spacings.

2. Results and Discussion

Scheme 1 shows the schematic synthetic processes of such ordered superlattice thin films. Water-soluble gold NC micelles were prepared by an interfacially driven microemulsion process^[19,29,31] using cetyltrimethyl ammonium bromide (CTAB) and *n*-dodecanethiol (*n*-DT)-derivatized gold NCs. *n*-DT-capped gold NCs were prepared according to the method of Brust et al.^[34] followed by heat treatment to narrow the gold NC size distribution to approximately 7% (see Scheme 1, step i).^[35] The thermodynamically favorable interdigitation between the *n*-DT and CTAB layers stabilizes the gold NC micelles in aqueous solution.^[30] Tetraethylorthosilicate (TEOS) was used as a precursor and was added to the above solution, followed by hydrolysis and condensation under acidic conditions at room temperature for 1 h. In addition to TEOS, bis(triethoxysilyl) ethane (BTEE) was used to tune the matrix composition within the superlattice films. Ordered superlattice thin films were prepared by spin-coating the above solution on substrates such as silicon wafers, glass, etc. (see Scheme 1, step ii). In order to study the siloxane condensation effect on the formation of an ordered superlattice, the above solution was aged at room temperature for different periods of time before spin-coating.

The gold/silica superlattice films have an average refractive index of ca. 1.7 and thicknesses of 100 to 300 nm depending on the spin rate. The film thickness can reach up to 25 μm when casting. Figure 1D shows an optical microscopy image of a red-



Scheme 1. Formation of water-soluble gold-NC micelles by surfactant/lipid encapsulation (i) and their self-assembly with soluble silica in a controlled sol-gel process (ii) into ordered gold NC/silica superlattice films through spin coating (iii); A) *n*-Dodecanethiol (*n*-DT)-stabilized, hydrophobic gold NCs; B) *n*-DT-stabilized gold NCs are encapsulated inside surfactant micelles by an interfacially driven oil-in-water microemulsion process [19]. C) Sol-gel self-assembly is conducted in acidic conditions; water-soluble oligomeric silica species preferentially interact with gold NC micelles and further self-assemble into fcc gold-NC superlattice films (D) upon drying (iii).

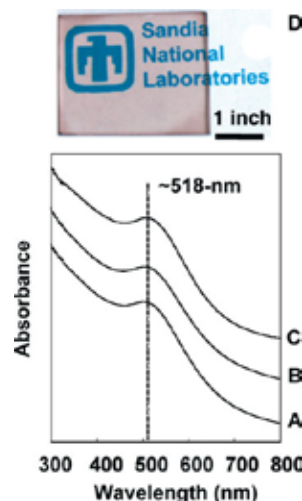


Figure 1. UV-vis spectra of A) *n*-DT-stabilized gold NCs, B) a gold-NC/silica superlattice film prepared using TEOS, and C) gold/ethyl bridged silsesquioxane film prepared using bis(triethoxysilyl) ethane. D) Optical microscopy image of as-prepared ordered gold/silica film on a glass substrate that covers the logo of Sandia National Laboratories (1 in = 2.54 cm).

H. Fan et al./3D-Ordered Gold Nanocrystal/Silica Superlattice Thin Films

dish film that exhibits very good optical transparency. Optical properties of the superlattice film were characterized using UV-vis spectroscopy, as shown in Figures 1A–C. The superlattice film exhibits a characteristic surface plasmon resonance band at ca. 518 nm, as expected from gold NCs. In comparison with the spectra of monodisperse *n*-DT-stabilized gold NCs, the position and width of the surface plasmon band from the gold superlattice film stays unchanged, suggesting that gold NCs inside the film remain monodisperse. This was further confirmed by TEM results (see below). Low-magnification scanning electron microscopy (SEM) imaging (Fig. 2A) shows that the film has a uniform and continuous surface without macroscopic granularity or cracks. Figure 2B shows a high-res-

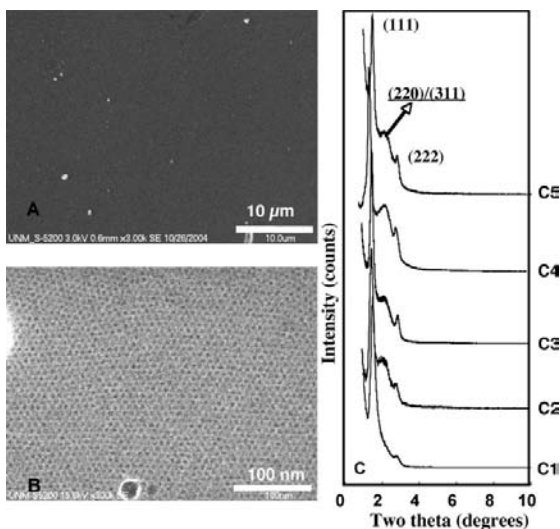


Figure 2. A) Low-resolution SEM image of ordered gold NC/silica superlattice thin film. B) High-resolution SEM image from the same specimen as in (A). C) X-ray diffraction patterns of gold NC/silica superlattice films. Ordered gold/silica film prepared using a coating solution that was aged under ambient conditions for 24 h (C1), and 5 h (C2). C3) Ordered gold/silica film prepared using a coating solution without aging. C4) Ordered gold/silsesquioxane film prepared using a solution that was aged under ambient conditions for 24 h. C5) Ordered gold/silsesquioxane film prepared using a solution without aging.

olution SEM image of the as-prepared film surface. Ordered gold NCs are distributed uniformly on the film surface.

Figure 2C3 shows a representative low-angle X-ray diffraction (XRD) pattern of a superlattice thin film prepared according to pathway i–iii (Scheme 1), using ca. 3 nm *n*-DT-stabilized gold NCs, CTAB, and TEOS. The patterns can be indexed as an fcc structure with unit cell $a \sim 10.5$ nm. The primary peaks are assigned as (111), (220)/(311), and (222) reflections. Figure 2C1 shows the XRD pattern of a film prepared using a spin solution aged at room temperature for 24 h. The film exhibits a lower degree of ordering, with the disappearance of the (220)/(311) and an intensity decrease of the (222) reflections. Figure 3A shows a representative cross-sectional TEM image of

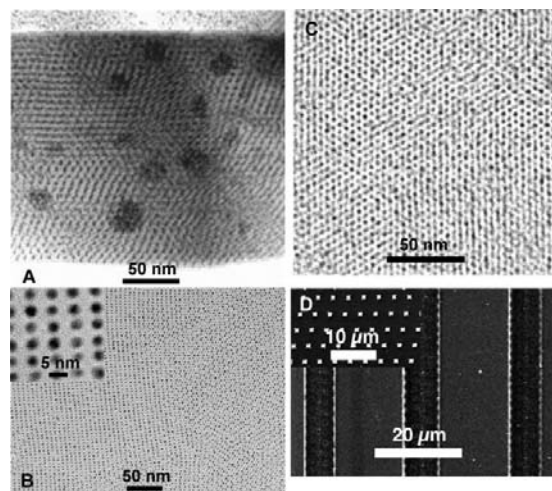


Figure 3. A) Cross-sectional TEM image of ordered gold NC/silica superlattice thin film. B) Representative plan-view TEM image of ordered gold NC/silica superlattice films through complete film thickness showing a seamless transition among three ordered domains [211] and [111]. Inset: a high-resolution TEM image. C) Representative plan-view TEM image of ordered gold NC/silsesquioxane superlattice films prepared using BTEE. D) Patterned gold NC/silica superlattice thin films fabricated by a micro-molding method [42]. Inset: square-dot patterns with smaller feature size.

an ordered superlattice film. Periodically ordered regions are observed throughout the whole film thickness. The sharp, continuous, and uniform air/film and film/substrate interfaces are consistent with the SEM results, showing no steps, kinks, or cracking, which appear in superlattice films prepared by evaporation of NC solutions.^[14,36,37] A representative plan-view TEM image is shown in Figure 3B. The TEM images are consistent with an fcc structure (*Fm3m* space group) with a measured unit cell $a \sim 10.8$ nm and a minimum average interparticle spacing of ca. 2.3 nm. Note that the gold NC/silica superlattice thin film has a larger unit cell than that of previous superlattice films and solids.^[38] This is due to the fact that here the gold NCs are arranged within a silica matrix. A thin silica layer exists between each individual gold NC. The silica insulating layer was further confirmed by a high-resolution TEM image (Fig. 3B, inset). As shown in the plan-view image (Fig. 3B), regions of ordered gold-NC arrays inside silica exhibit no preferred orientation, with a seamless transition between the ordered domains of gold NCs. Within the film, the gold NCs remain monodisperse, which is consistent with UV-vis results (see Fig. 1).

The formation of ordered gold NC/silica thin films is analogous to that of the self-assembly of surfactant and silica. Charge interactions and hydrogen bonding between hydrolyzed silica and surfactant head groups on the NC-micelle surface drive the formation of an ordered gold NC/silica mesophase.^[39] However, the two systems exhibit a distinct tendency to form mesostructures. Prior work on the self-assembly of

pure surfactant and silica indicated that a series of mesostructures can be formed, including lamellar, 1D hexagonal, cubic, and 3D hexagonal periodic symmetries.^[39] In the case of the self-assembly of NC micelles and silica, only fcc mesostructures are preferentially formed, regardless of the basic and acidic catalytic conditions. This is probably due to the fact that the gold NC micelles are preformed in a homogeneous solution and behave rather like a “hard” sphere, tending to form close packing, rather than “soft” pure surfactant micelles, which are inclined to undergo phase transformation. Vital to the formation of transparent, ordered gold-NC/silica superlattice films is the use of stable and homogeneous spinning or casting solutions that, upon evaporation of water, undergo self-assembly of NC micelles and soluble silica. For this purpose, we prepared oligomeric silica sols in NC micelle aqueous solution with a low hydronium ion concentration (ca. pH2), which were designed to minimize the siloxane condensation rate and thereby enable facile silica and NC micelle self-assembly during spin-coating or casting.^[32] The aging experiments (Fig. 2C1–3) unambiguously demonstrate that extensive silica condensation, which results in polymeric silica species, does not favor self-assembly, leading to a less-ordered film. The method is flexible, and allows the tuning of framework composition, and thus the dielectric (*k*) properties, by using different sol-gel precursors. Organo-bridged silsesquioxane is an ideal, low-*k* host, exhibiting chemical and mechanical robustness.^[40,41] In addition to silica, we have demonstrated the synthesis of ordered gold-NC arrays inside an organosilsesquioxane framework. The ordered gold-NC/silsesquioxane was prepared using ~3 nm *n*-DT-stabilized gold NCs, CTAB, and BTEE. The corresponding XRD patterns (Fig. 2C4,5) and TEM image (Fig. 3C) reveal that these films exhibit an ordered fcc mesostructure. In addition, we observed from the XRD results that, when using BTEE, the self-assembly is not strongly affected by solution aging, unlike the case when using TEOS. This is due to the fact that the organo-bridged precursor has a relatively slower hydrolysis and condensation rate than TEOS.^[33]

The ability to form patterned films is essential for device fabrication. A homogeneous solution of gold-NC micelles allows the use of several soft-lithographic techniques, such as micro-molding, pen writing, and inkjet printing, to pattern the ordered gold-NC/silica superlattice films.^[41] We have demonstrated the formation of patterned gold-NC/silica superlattice films based on our previous work on patterning surfactant-templated silica mesophases. Figure 3D shows patterned stripes and dots containing ordered gold-NC/silica superlattices fabricated using micro-molding techniques.^[42] The pattern sizes are determined by the feature sizes of the poly(dimethylsiloxane) (PDMS) stamps.

In comparison to previous methods for assembling NC superlattices by the evaporation of a colloidal solution of NCs, our method provides several advantages. First, unlike previous superlattice films formed by the evaporation of organic flammable solutions, the water-soluble gold-NC micelles allow superlattice films to be fabricated in water, resulting in enhanced safety and better compatibility with current semiconductor-fabrication processing. Second, by using different sol-

gel precursors, our method allows simple tuning of framework composition, and thus dielectric properties, between the gold NCs. This is essential for achieving enhanced collective properties in such 3D superlattice films.^[17,18] Furthermore, the inorganic framework provides chemical and mechanical robustness and prevents films from cracking, which is important for device fabrication. It is believed that the formation of an NC superlattice by organic solvent evaporation is an entropy-driven process in which NCs organize in such a way as to achieve the highest packing density or maximum entropy.^[2,12,14,43] In our method, silica condensation affects ordering during formation of gold-NC/silica superlattice films. It is interesting to note that previous methods of assembling NCs during solvent evaporation led to two-level preferential orientations. First, the ordered NCs pack as an fcc structure with (111) planes parallel to substrates.^[13,14] Second, the crystal structure of each individual NC is also orientated relative to the substrate.^[13] In our system, the films consist of ordered “domains” randomly distributed throughout the film. From wide-angle XRD, we observed no preferred orientation of gold crystal structure relative to the substrate.

3. Conclusions

We have developed a simple and general method to synthesize ordered, 3D, transparent gold-NC/silica superlattice thin films using self-assembly of water-soluble gold NC-micelles and soluble silica by spin-coating. The self-assembly process allows the facile tuning of the host-matrix composition by using different sol-gel precursors, and provides compatibility with standard microelectronics processing/patterning, enabling higher temperature operation. Acidic sol-gel chemistry ensures spin-solution homogeneity and stability, facilitating the self-assembly of soluble silica and NC micelles into ordered, transparent gold-NC/silica films. The ease of preparing semi-conducting and magnetic NC micelles using an interfacially driven microemulsion process makes it possible to synthesize ordered quantum dot/metal oxide and magnetic NC/metal oxide arrays, and to integrate them into laser and memory devices.^[30,31] The robust, 3D NC/silica superlattice films are of interest for the development of collective optical and electronic phenomena, and, importantly, for the integration of NC arrays into device architectures.^[8,44] Ultimately, the ordered gold/silica superlattice films are ideal platforms for the fabrication of molecular electronic nanodevices^[45] and surface-enhanced Raman spectroscopy (SERS)-based chemical and biosensors.^[20,46]

4. Experimental

Synthesis of Gold NCs: *n*-Dodecanethiol-modified gold NCs were synthesized using the method developed by Brust et al. [34]. An aqueous solution (60 mL) containing HAuCl₄ (0.7 g, Aldrich) was mixed with a solution of tetraoctylammonium bromide (4 g, Aldrich) in toluene (160 mL). The two-phase mixture was vigorously stirred until the tetrachloroaurate was transferred completely into the organic layer (judged by color changes: the aqueous phase became colorless and the

H. Fan et al./3D-Ordered Gold Nanocrystal/Silica Superlattice Thin Films

organic phase became dark yellow). *n*-Dodecanethiol (0.34 g, Aldrich) was added to the organic phase. A freshly prepared aqueous solution (40 mL) of sodium borohydride (0.78 g, Aldrich) was added slowly, with vigorous stirring; the reaction was complete after 20 min. After further stirring for 2 h, the organic phase was separated and evaporated in a rotary evaporator. Heat treatment at 140 °C was performed for 30–45 min [35]. The gold NCs were then purified by two cycles of precipitation, followed by size-selective precipitation using the solvent/non-solvent pair of toluene/ethanol. In general, the gold NCs were dissolved in toluene (10 mL) and precipitated using ethanol (50 mL).

Synthesis of Gold-NC Micelles: In a general preparation of water-soluble gold-NC micelles, a chloroform gold-NC solution (3 mL) containing *n*-dodecanethiol-stabilized gold NCs (0.35 g) was added to deionized water (8–12 g) containing CTAB (0.2 g) under vigorous stirring, to form a solution. The chloroform was removed by quick heating to transfer the hydrophobic gold NCs into the aqueous phase by encapsulation. A dark-colored solution (stock solution) was finally obtained and centrifuged at 2000 rpm for 5 min to remove any precipitate.

Gold NC/Silica Superlattice Thin Films: TEOS (0.08 g) or BTEE was added to the above stock solution (1 mL), followed by the addition of aqueous HCl solution (0.07 N or 1 N, 0.05 mL). The mixture was stirred for 1 h at room temperature. Superlattice films were formed by spin-coating at 500–2000 rpm. Aging studies were performed at room temperature for the desired time.

Characterization: The XRD spectra were used to characterize the 3D ordered arrays (film), and were recorded on a Siemens D500 diffractometer using Ni-filtered Cu K α radiation with $\lambda = 1.54 \text{ \AA}$ in θ - 2θ ($2\theta = 1$ – 10°) scan mode using a step size ranging from 0.02 and a dwell time of 2 s. TEM images were taken using a JEOL 2010 high-resolution microscope equipped with a Gatan slow-scan charge-coupled device (CCD) camera and operated at 200 keV. SEM images were taken with a Hitachi S-5200 FEG high-resolution microscope.

Received: September 7, 2005

Final version: October 11, 2005

Published online: March 23, 2006

- [1] A. P. Alivisatos, *Science* **1996**, 271, 933.
- [2] M. A. El-Sayed, *Acc. Chem. Res.* **2001**, 34, 257.
- [3] B. Dubertret, P. Skourides, D. J. Norris, V. Noireaux, A. H. Brivanlou, A. Libchaber, *Science* **2002**, 298, 1759.
- [4] Y. G. Sun, Y. N. Xia, *Science* **2002**, 298, 2176.
- [5] Y. D. Yin, R. M. Rioux, C. K. Erdonmez, S. Hughes, G. A. Somorjai, A. P. Alivisatos, *Science* **2004**, 304, 711.
- [6] S. H. Sun, C. B. Murray, D. Weller, L. Folks, A. Moser, *Science* **2000**, 287, 1989.
- [7] R. P. Andres, J. D. Bielefeld, J. I. Henderson, D. B. Janes, V. R. Kolagunta, C. P. Kubiak, W. J. Mahoney, R. G. Osifchin, *Science* **1996**, 273, 1690.
- [8] C. T. Black, C. B. Murray, R. L. Sandstrom, S. H. Sun, *Science* **2000**, 290, 1131.
- [9] C. P. Collier, R. J. Saykally, J. J. Shiang, S. E. Henrichs, J. R. Heath, *Science* **1997**, 277, 1978.
- [10] R. Doty, H. Yu, C. Shih, B. Korgel, *J. Phys. Chem. B* **2001**, 105, 8291.
- [11] M. Pileni, *J. Phys. Chem. B* **2001**, 105, 3358.
- [12] C. Murray, C. Kagan, M. Bawendi, *Annu. Rev. Mater. Sci.* **2000**, 30, 545.
- [13] C. B. Murray, C. R. Kagan, M. G. Bawendi, *Science* **1995**, 270, 1335.
- [14] M. B. Sigman, A. E. Saunders, B. A. Korgel, *Langmuir* **2004**, 20, 978.
- [15] D. V. Talapin, E. V. Shevchenko, A. Kornowski, N. Gaponik, M. Haase, A. L. Rogach, H. Weller, *Adv. Mater.* **2001**, 13, 1868.
- [16] D. V. Talapin, E. V. Shevchenko, C. B. Murray, A. Kornowski, S. Forster, H. Weller, *J. Am. Chem. Soc.* **2004**, 126, 12984.
- [17] J. Lee, V. C. Sundar, J. R. Heine, M. G. Bawendi, K. F. Jensen, *Adv. Mater.* **2000**, 12, 1102.
- [18] M. A. Petruska, A. V. Malko, P. M. Voyles, V. I. Klimov, *Adv. Mater.* **2003**, 15, 610.
- [19] H. Y. Fan, K. Yang, D. Boye, T. Sigmon, K. Malloy, H. Xu, G. P. Lopez, C. Brinker, *Science* **2004**, 304, 567.
- [20] H. Y. Fan, Y. Q. Zhou, G. P. Lopez, *Adv. Mater.* **1997**, 9, 728.
- [21] M. Epifani, C. Giannini, L. Tapfer, L. Vasanelli, *J. Am. Ceram. Soc.* **2000**, 83, 2385.
- [22] D. K. Sarkar, F. Cloutier, M. A. El Khakani, *J. Appl. Phys.* **2005**, 97, 084302.
- [23] A. Fukuoka, H. Araki, J. Kimura, Y. Sakamoto, T. Higuchi, N. Sugimoto, S. Inagaki, M. Ichikawa, *J. Mater. Chem.* **2004**, 14, 752.
- [24] Y. Guari, C. Theuleux, A. Mehdi, C. Reye, R. J. P. Corriu, S. Gomez-Gallardo, K. Philippot, B. Chaudret, R. Dutartre, *Chem. Commun.* **2001**, 1374.
- [25] Y. Guari, C. Theuleux, A. Mehdi, C. Reye, R. J. P. Corriu, S. Gomez-Gallardo, K. Philippot, B. Chaudret, *Chem. Mater.* **2003**, 15, 2017.
- [26] F. J. Brieler, M. Froba, L. M. Chen, P. J. Klar, W. Heimbrodt, H. A. K. von Nidda, A. Loidl, *Chem. Eur. J.* **2002**, 8, 185.
- [27] A. T. Cho, J. M. Shieh, J. Shieh, Y. F. Lai, B. T. Dai, F. M. Pan, H. C. Kuo, Y. C. Lin, K. J. Chao, P. H. Liu, *Electrochem. Solid-State Lett.* **2005**, 8, G143.
- [28] H. Zeng, J. Li, J. P. Liu, Z. L. Wang, S. H. Sun, *Nature* **2002**, 420, 395.
- [29] H. Y. Fan, Z. Chen, C. Brinker, J. Clawson, T. Alam, *J. Am. Chem. Soc.* **2005**, 127, 13746.
- [30] H. Y. Fan, E. Leve, J. Gabaldon, A. Wright, R. Haddad, C. J. Brinker, *Adv. Mater.* **2005**, 17, 2587.
- [31] H. Y. Fan, E. W. Leve, C. Scullin, J. Gabaldon, D. Tallant, S. Bunge, T. Boyle, M. C. Wilson, C. J. Brinker, *Nano Lett.* **2005**, 5, 645.
- [32] C. J. Brinker, Y. F. Lu, A. Sellinger, H. Y. Fan, *Adv. Mater.* **1999**, 11, 579.
- [33] C. J. Brinker, G. W. Scherer, *Sol-Gel Science: The Physics and Chemistry of Sol-Gel Processing*, Academic Press, San Diego, CA **1990**.
- [34] M. Brust, M. Walker, D. Bethell, D. J. Schiffrin, R. Whyman, *Chem. Commun.* **1994**, 801.
- [35] M. Maye, W. Zheng, F. Leibowitz, N. Ly, C. Zhong, *Langmuir* **2000**, 16, 490.
- [36] S. Chen, *Langmuir* **2001**, 17, 2878.
- [37] C. B. Murray, C. R. Kagan, M. G. Bawendi, *Annu. Rev. Mater. Sci.* **2000**, 30, 577.
- [38] Z. L. Wang, *Adv. Mater.* **1998**, 10, 13.
- [39] Q. S. Huo, D. I. Margolese, U. Ciesla, P. Y. Feng, T. E. Gier, P. Sieger, R. Leon, P. M. Petroff, F. Schuth, G. D. Stucky, *Nature* **1994**, 368, 317.
- [40] Y. F. Lu, H. Y. Fan, N. Doke, D. A. Loy, R. A. Assink, D. A. LaVan, C. J. Brinker, *J. Am. Chem. Soc.* **2000**, 122, 5258.
- [41] H. Y. Fan, Y. F. Lu, A. Stump, S. T. Reed, T. Baer, R. Schunk, V. Perez Luna, G. P. Lopez, C. J. Brinker, *Nature* **2000**, 405, 56.
- [42] Y. N. Xia, J. A. Rogers, K. E. Paul, G. M. Whitesides, *Chem. Rev.* **1999**, 99, 1823.
- [43] B. Korgel, N. Zaccaroni, D. Fitzmaurice, *J. Am. Chem. Soc.* **1999**, 121, 3533.
- [44] A. Courty, A. Mermet, P. Albouy, E. Duval, M. Pileni, *Nat. Mater.* **2005**, 4, 395.
- [45] J. Chen, W. Wang, J. Klemic, M. A. Reed, B. W. Axelrod, D. M. Kaschak, A. M. Rawlett, D. W. Price, S. M. Dirk, J. M. Tour, D. S. Grubisha, D. W. Bennett, in *Molecular Electronics II* (Eds: A. Aviram, M. Ratner, V. Mujica), Annals of the New York Academy of Sciences, Vol. 960, New York Academy of Sciences, New York **2002**, p. 69.
- [46] Y. W. C. Cao, R. C. Jin, C. A. Mirkin, *Science* **2002**, 297, 1536.

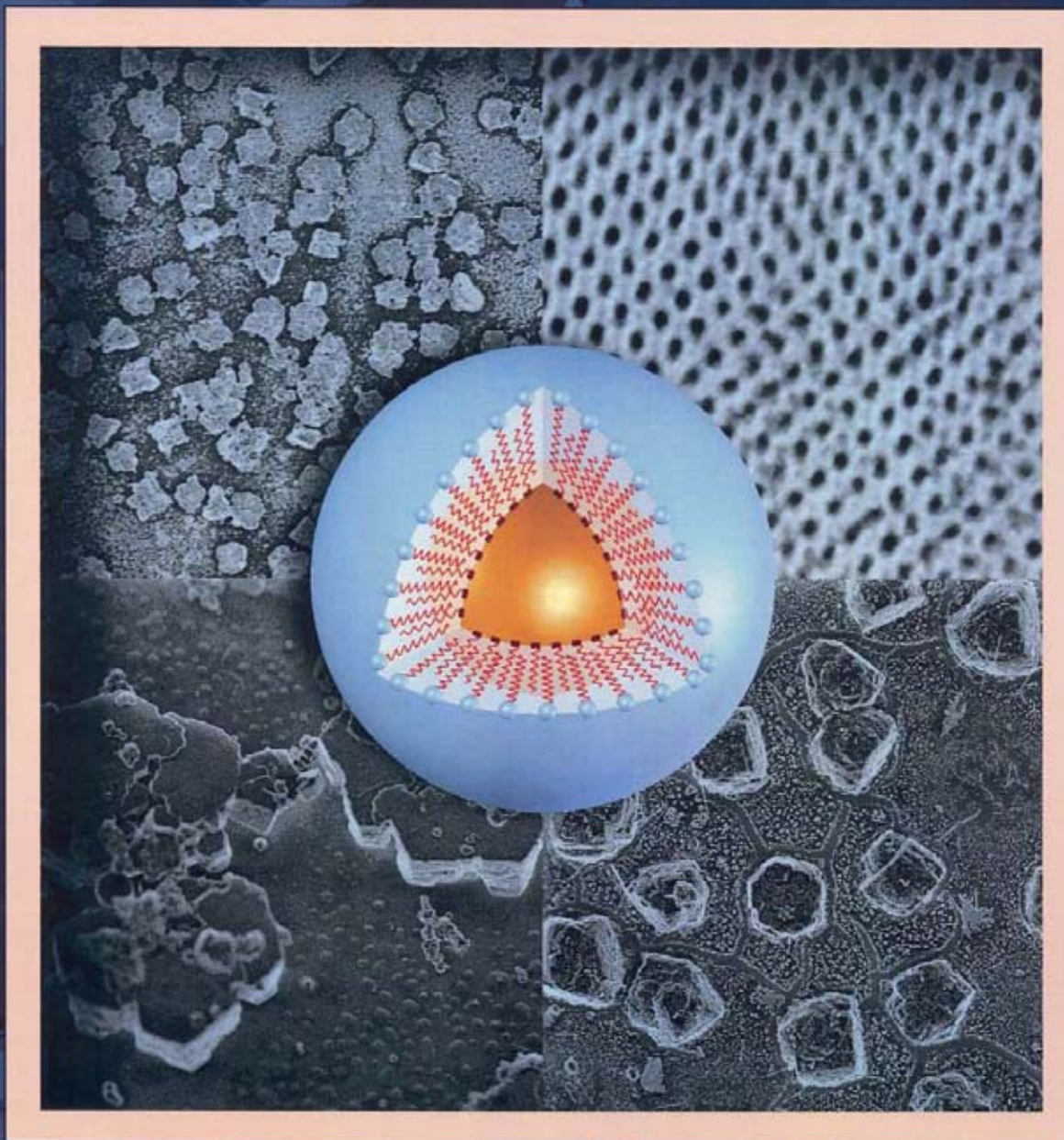
Appendix D: Featured scientific journal publications/cover articles.

SELF-ASSEMBLING PROCESS *for*
FABRICATING TAILORED THIN FILMS

CHEMISTRY OF MATERIALS

SEPTEMBER 5, 2006
VOLUME 18 NUMBER 18

A PUBLICATION OF THE AMERICAN CHEMICAL SOCIETY



<http://pubs.acs.org/cm>

Hierarchically Organized Nanoparticle Mesostructure Arrays Formed through Hydrothermal Self-Assembly

Adam Wright,[†] John Gabaldon,[†] D. Bruce Burckel,[‡] Ying-Bing Jiang,[†] Z. Ryan Tian,^{‡,§} Jun Liu,^{‡,||} C. Jeffrey Brinker,^{†,‡} and Hongyou Fan^{*,†,‡}

Chemical Synthesis and Nanomaterials Department, Sandia National Laboratories, Albuquerque, New Mexico 87106, and Department of Chemical and Nuclear Engineering, The University of New Mexico/NSF Center of Micro-Engineered Materials, Albuquerque, New Mexico 87131

Received March 10, 2006. Revised Manuscript Received May 3, 2006

We report a new self-assembly pathway that leads to supported and hierarchically organized gold nanoparticle mesostructure arrays on solid substrates such as glass slide, thermal oxide, photopolymer film, and mica. Using the nanoparticle micelle as a building block, hierarchical gold nanoparticle mesostructure arrays were prepared by a hydrothermal nucleation and growth process through self-assembly of nanoparticle micelles and organosilicates under basic conditions. Depending on the substrates used, the shape, order, and orientation of the gold nanoparticle mesostructure during nucleation and growth exhibit distinct features. Transmission electron microscopy and X-ray diffraction results revealed that gold nanoparticles were organized as a face-centered cubic mesostructure with precisely controlled interparticle spacing. Optical characterization using UV–vis spectroscopy shows a characteristic surface plasmon resonance band resulted from the ordered nanoparticle arrays. This method provides new means for colloidal self-assembly and for the fabrication of platforms for surface enhanced Raman scattering-based sensors and electric and optical nanodevices with enhanced thermal, chemical, and mechanical robustness.

Introduction

Synthesis of hierarchically structured materials holds both fundamental and practical importance in optical, electronic, and magnetic devices,^{1–6} catalysis and sorption,⁷ optical elements,⁸ and sensors.^{2,3} Prior fabrication efforts include biomimetic,^{9–11} self-similar,¹² soft lithography,¹³ and rapid printing¹⁴ methods. Recently, more progress has been made

in the synthesis of hierarchically ordered nanoparticle/polymer macrostructures through interfacially driven self-assembly of polymers with metal and semiconductor nanoparticles.^{15–18} However, it has been recently suggested that it is desirable to synthesize ordered nanoparticle arrays inside inorganic matrixes that provide thermal, chemical, and mechanical robustness needed for enhanced device performance.^{3,19,20} Earlier efforts have focused on encapsulation of metal nanoparticles inside sol–gel matrixes through introduction of metal nanoparticles²¹ or metal precursors followed by either thermally decomposing or reducing them.^{22,23} Recently, mesoporous materials have been used as templates to create hybrid silica materials loaded with metal or semiconducting nanoparticles or nanowires through

* To whom correspondence should be addressed. E-mail: hfan@sandia.gov.

[†] The University of New Mexico/NSF Center of Micro-Engineered Materials

[‡] Sandia National Laboratories

[§] Current address: Department of Chemistry, University of Arkansas, Fayetteville, AR 72701.

^{||} Current address: Pacific Northwest National Laboratory, 902 Battelle Boulevard, K2-50, Box 999, Richland, WA 99352.

- (1) Black, C. T.; Murray, C. B.; Sandstrom, R. L.; Sun, S. H. *Science* **2000**, *290* (5494), 1131.
- (2) Cao, Y. W. C.; Jin, R. C.; Mirkin, C. A. *Science* **2002**, *297* (5586), 1536.
- (3) Fan, H. Y.; Yang, K.; Boye, D.; Sigmon, T.; Malloy, K.; Xu, H.; Lopez, G. P.; Brinker, C. *Science* **2004**, *304* (5670), 567–571.
- (4) Pileni, M. P. *J. Phys. Chem. B* **2001**, *105* (17), 3358.
- (5) Zeng, H.; Li, J.; Liu, J. P.; Wang, Z. L.; Sun, S. H. *Nature* **2002**, *420* (6914), 395.
- (6) Xia, Y. N.; Halas, N. J. *MRS Bull.* **2005**, *30* (5), 338.
- (7) Dai, S. *Chem.–Eur. J.* **2001**, *7* (4), 763.
- (8) Yang, P. D.; Wirthsberger, G.; Huang, H. C.; Cordero, S. R.; McGehee, M. D.; Scott, B.; Deng, T.; Whitesides, G. M.; Chmelka, B. F.; Buratto, S. K.; Stucky, G. D. *Science* **2000**, *287* (5452), 465.
- (9) Aizenberg, J.; Weaver, J. C.; Thanawala, M. S.; Sundar, V. C.; Morse, D. E.; Fratzl, P. *Science* **2005**, *309* (5732), 275.
- (10) Aksay, I.; Trau, M.; Manne, S.; Honma, I.; Yao, N.; Zhou, L.; Fenter, P.; Eisenberger, P.; Gruner, S. *Science* **1996**, *273* (5277), 892–898.
- (11) Mann, S.; Ozin, G. A. *Nature* **1996**, *382* (6589), 313.
- (12) Tian, Z. R. R.; Liu, J.; Voigt, J. A.; McKenzie, B.; Xu, H. F. *Angew. Chem., Int. Ed.* **2003**, *42* (4), 414.
- (13) Yang, P. D.; Deng, T.; Zhao, D. Y.; Feng, P. Y.; Pine, D.; Chmelka, B. F.; Whitesides, G. M.; Stucky, G. D. *Science* **1998**, *282* (5397), 2244–2246.

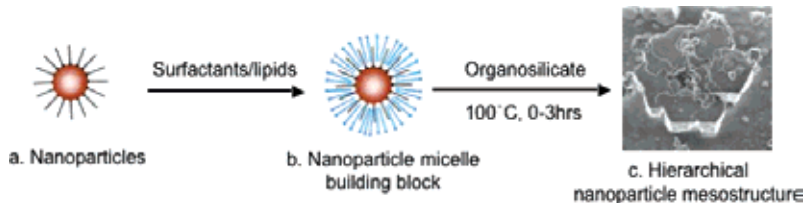
- (14) Fan, H. Y.; Lu, Y. F.; Stump, A.; Reed, S. T.; Baer, T.; Schunk, R.; Perez-Luna, V.; Lopez, G. P.; Brinker, C. J. *Nature* **2000**, *405* (6782), 56.
- (15) Boker, A.; Lin, Y.; Chiapperini, K.; Horowitz, R.; Thompson, M.; Carreon, V.; Xu, T.; Abetz, C.; Skaff, H.; Dinsmore, A. D.; Emrick, T.; Russell, T. P. *Nat. Mater.* **2004**, *3* (5), 302.
- (16) Lin, Y.; Boker, A.; He, J. B.; Sill, K.; Xiang, H. Q.; Abetz, C.; Li, X. F.; Wang, J.; Emrick, T.; Long, S.; Wang, Q.; Balazs, A.; Russell, T. P. *Nature* **2005**, *434* (7029), 55.
- (17) Lopes, W. A.; Jaeger, H. M. *Nature* **2001**, *414* (6865), 735.
- (18) Saunders, A. E.; Shah, P. S.; Sigman, M. B.; Hanrath, T.; Hwang, H. S.; Lim, K. T.; Johnston, K. P.; Korgel, B. A. *Nano Lett.* **2004**, *4* (10), 1943.
- (19) Petruska, M. A.; Malko, A. V.; Voyles, P. M.; Klimov, V. I. *Adv. Mater.* **2003**, *15* (7–8), 610–613.
- (20) Sundar, V. C.; Eisler, H. J.; Bawendi, M. G. *Adv. Mater.* **2002**, *14* (10), 739.
- (21) Fan, H. Y.; Zhou, Y. Q.; Lopez, G. P. *Adv. Mater.* **1997**, *9* (9), 728.
- (22) Epifani, M.; Giannini, C.; Tapfer, L.; Vasaneli, L. *J. Am. Ceram. Soc.* **2000**, *83* (10), 2385.
- (23) Sarkar, D. K.; Cloutier, F.; El Khakani, M. A. *J. Appl. Phys.* **2005**, *97* (8), 084302.

Appendix D: Featured scientific journal publications/cover articles.

SELF-ASSEMBLING PROCESS for FABRICATING TAILORED THIN FILMS

Nanoparticle Mesostructure Arrays

Chem. Mater., Vol. 18, No. 13, 2006 3035

Scheme 1. Formation of the Water-Soluble Nanoparticle Micelle and Preparation of Hierarchical Nanoparticle Mesostructure Arrays through Hydrothermal Self-Assembly of Water-Soluble Nanoparticle Micelle Building Blocks with Organosilicate^a

^a (a) Organic monolayer capped, hydrophobic gold nanoparticles. (b) Nanoparticle micelle building blocks are formed through evaporation-driven transfer of hydrophobic nanoparticles into the interior of surfactant/lipid micelles in an interfacially mediated oil-in-water microemulsion process. (c) Hierarchical nanoparticle mesostructure arrays are formed via a hydrothermal self-assembly process.

infiltration of precursor solutions followed by chemical or electrochemical reduction or direct infiltration of nanoparticles.^{24–28} Several disadvantages for the above methods include the following: First, the nanoparticle arrays inside the final materials exhibit poorly defined or less-ordered structure. This is problematic for the fundamental studies of charge transport to get reproducible results. Second, the methods have less control over particle sizes and loading. Third, it is difficult for the above methods to precisely control interparticle spacing that is essential for achieving new physical properties resulting from coupling between neighboring nanoparticles.^{5,29,30} Finally, as a result of the unconnected pore channel or dead pore within the porous materials that causes transport problems during infiltration, the resulting materials exhibited vacant areas that were not completely filled with nanoparticles or nanowires.

Here we report a new self-assembly pathway that leads to supported hierarchically ordered gold nanoparticle/organosilicate mesostructure arrays on a glass slide, thermal oxide, a photopolymer film, and mica. Using the nanoparticle micelle as a building block, hierarchically ordered nanoparticle mesostructure arrays were prepared by a hydrothermal nucleation and growth process through self-assembly of nanoparticle micelles and organosilicates under basic conditions. Gold nanoparticles were organized as a face-centered cubic (fcc) mesostructure with precisely controlled interparticle spacing. Depending on the substrates used, the shape, order, and orientation of mesostructures during nucleation and growth exhibit distinct features. The surface plasmon resonance in the visible region resulting from the ordered gold nanoparticle arrays suggests the potential applications for surface enhanced Raman scattering (SERS)-

based sensors² and electric and optical nanodevices with enhanced thermal, chemical, and mechanical robustness.^{18,19}

Experimental Section

All materials were ordered through Aldrich without further purifications.

Sample Preparation. Gold nanoparticles were prepared according to the method reported by Brust et al.⁴⁰ using dodecanethiol (1-DT) as a stabilizing ligand. Before precipitation of 1-DT-stabilized gold nanoparticles, toluene was first evaporated at 40 °C under vacuum. The resulting waxy black product was then heat treated at 140 °C for 0.5 h. This heat treatment process enables Oswald ripening and allows reorganization in nanoparticle size, leading to much narrower nanoparticle size distribution (~7%), which is essential to form ordered nanoparticle crystal arrays. Gold nanoparticle micelles were synthesized according to previous work.^{3,31–33} A total of 0.1 g of sodium hydroxide was added to 9 mL of gold nanoparticle micelle aqueous solution followed by adding 0.28 g of bis(triethoxysilyl)ethane (BTEE) in a 20 mL vial. After the solution was stirred for 1 h at room temperature, glass slides or fresh-peeled mica were placed vertically inside these vials. After they were sealed, the vials were placed vertically inside an oven at 100 °C for 0–3 h. The slides were then taken out and rinsed by deionized water and dried.

Characterizations. The X-ray diffraction (XRD) spectra were recorded on a Siemens D500 diffractometer using Ni-filtered Cu K α radiation with $\lambda = 1.54 \text{ \AA}$ in $\theta-2\theta$ ($2\theta = 1-10^\circ$) scan mode using a step size ranging from 0.02° and dwell time of 2 s. Transmission electron microscopy (TEM) images were taken at JEOL 2010 high-resolution microscope equipped with Gatan slow scan charge-coupled device camera and operated at 200 keV. Scanning electron microscopy (SEM) images were taken using Hitachi 5200 microscope.

Results and Discussion

The self-assembly process (shown in Scheme 1) involves two steps: (1) preparation of a building block solution and (2) hydrothermal nucleation and growth of nanoparticle

- (24) Fukuoka, A.; Araki, H.; Kimura, J.; Sakamoto, Y.; Higuchi, T.; Sugimoto, N.; Inagaki, S.; Ichikawa, M. *J. Mater. Chem.* **2004**, *14* (4), 752.
- (25) Guari, Y.; Theiuleux, C.; Mehdi, A.; Reye, C.; Corriu, R. J. P.; Gomez-Gallardo, S.; Philippot, K.; Chaudret, B.; Dutartre, R. *Chem. Commun.* **2001** (15), 1374.
- (26) Guari, Y.; Theiuleux, C.; Mehdi, A.; Reye, C.; Corriu, R. J. P.; Gomez-Gallardo, S.; Philippot, K.; Chaudret, B. *Chem. Mater.* **2003**, *15* (10), 2017.
- (27) Brieler, F. J.; Froba, M.; Chen, L. M.; Klar, P. J.; Heimbrodt, W.; von Nidda, H. A. K.; Loidl, A. *Chem.—Eur. J.* **2002**, *8* (1), 185.
- (28) Cho, A. T.; Shieh, J. M.; Shieh, J.; Lai, Y. F.; Dai, B. T.; Pan, F. M.; Kuo, H. C.; Lin, Y. C.; Chao, K. J.; Liu, P. H. *Electrochem. Solid State Lett.* **2005**, *8* (6), G143.
- (29) Collier, C. P.; Saykally, R. J.; Shiang, J. J.; Henrichs, S. E.; Heath, J. R. *Science* **1997**, *277* (5334), 1978–1981.
- (30) Pileni, M. J. *Phys. Chem. B* **2001**, *105*, 3358.

- (31) Fan, H. Y.; Leve, E. W.; Scullin, C.; Gabaldon, J.; Tallant, D.; Bunge, S.; Boyle, T.; Wilson, M. C.; Brinker, C. J. *Nano Lett.* **2005**, *5* (4), 645.
- (32) (a) Fan, H. Y.; Leve, E.; Gabaldon, J.; Wright, A.; Haddad, R.; Brinker, C. *Adv. Mater.* **2005**, *17*, 2587–2590. (b) Fan, H. Y.; Wright, A.; Gabaldon, J.; Rodriguez, A.; Brinker, C. J.; Jiang, Y. B. *Adv. Funct. Mater.* **2006**, *16*, 891–895. (c) Fan, H. Y.; Gabaldon, J.; Brinker, C. J.; Jiang, Y. B. *Chem. Commun.* **2006**, *22*, 2323–2325.
- (33) Fan, H. Y.; Chen, Z.; Brinker, C.; Clawson, J.; Alam, T. J. *Am. Chem. Soc.* **2005**, *127*, 13746–13747.

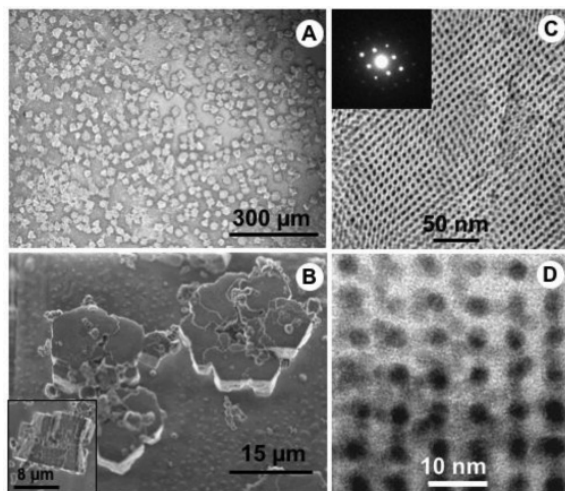


Figure 1. Representative SEM and TEM micrographs of hierarchical nanoparticle mesostructure arrays on glass slides. (A) Sample was prepared on an amorphous glass slide using BTEE as the precursor under basic conditions at 100 °C for 60 min. (B) A magnified SEM image of (A) showing that the hierarchical mesostructure consists of three to five subunits. The inset shows a cross-sectional image of a main unit of the hierarchical mesostructure indicating that the crystal height is $\sim 8 \mu\text{m}$. Representative TEM images from [110] orientation (C) and [100] orientation (D). Inset in part C shows the selected area electron diffraction pattern from the image in part C and suggests the three-dimensionally ordered features.

mesostructures. In the first step, the nanoparticle micelles were synthesized through a surfactant encapsulation process^{3,31–33} using 1-DT capped gold nanoparticles and cetyltrimethylammonium bromide (CTAB; Scheme 1a). Briefly, a monodisperse, DT-capped gold nanoparticle chloroform solution was added to a CTAB aqueous solution to form an oil-in-water microemulsion under vigorous stirring. The highly volatile chloroform was then removed by heating at $\sim 40 \text{ }^\circ\text{C}$ for ~ 10 min. Evaporation of the chloroform induces transfer of DT-capped, hydrophobic gold nanoparticles into the hydrophobic core of surfactant micelles through van der Waals interactions between the interdigitated alkane chains of DT and CTAB, forming water-soluble gold nanoparticle micelles. The second step involves the nucleation and growth of nanoparticle mesostructure arrays in a hydrothermal self-assembly process (Scheme 1b). BTEE was chosen as the precursor for its preferential self-assembly with the micellar interface and formation of well-controlled external topology.^{12,34} In a typical synthesis, BTEE and sodium hydroxide are mixed with a nanoparticle micelle aqueous solution in a small vial (see Experimental Section). After 1 h of stirring at room temperature, a substrate such as a microscope slide, thermal oxide coated silicon wafer, or fresh-peeled mica slide was vertically placed inside the small vial. The vials were then sealed and placed inside an oven at 100 °C for crystal growth.

Well-shaped and oriented nanoparticle mesostructure arrays began to grow over several hours. These large nanoparticle mesostructures covered the whole substrate. Figure 1 shows a typical SEM micrograph of large area

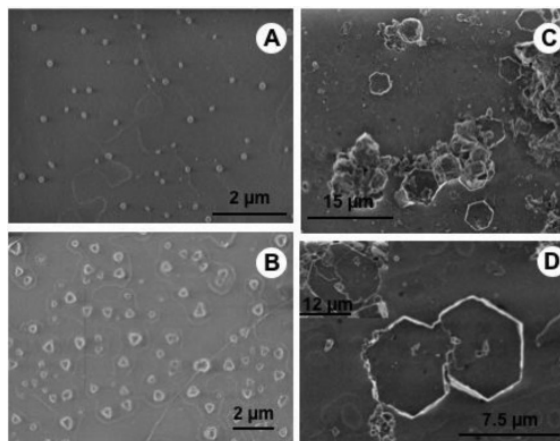


Figure 2. SEM micrographs of samples at different growth times. Results suggest that hierarchical nanoparticle mesostructure arrays are formed through a heterogeneous nucleation and growth process on glass slides. (A) At 10 min, $\sim 0.3 \mu\text{m}$ particles were observed. (B) At 20 min, crystals with triangular shape were observed. (C, D) At 40 min, a single subunit and some intermediate hierarchical structures have been formed.

arrays of the nanoparticle mesostructures grown on glass slides. They are fairly uniform in shape and size ($\sim 15 \mu\text{m}$, Figure 1A) with well-defined external topology. The high-resolution SEM image (Figure 1B) shows that each individual main unit exhibits flowerlike hierarchical structure, which consists of three to five subunits with hexagonal shape and size of $\sim 7 \mu\text{m}$. A cross-sectional view of the main unit (Figure 1B, inset) shows a height of about $8 \mu\text{m}$. The TEM image (Figure 1C,D) and low-angle XRD patterns (Figure 4) reveal that the gold nanoparticles self-assemble as a fcc mesostructure inside the BTEE matrix. Figure 1C,D shows representative TEM images of [110] and [100] orientations of the nanoparticle mesostructure along with its corresponding selected area electron diffraction pattern. The TEM images are consistent with a unit cell of $\sim 10.6 \text{ nm}$ and a uniform, minimum interparticle spacing of $\sim 3 \text{ nm}$.

To study the formation mechanism, samples at different growth times were examined by SEM (Figure 2) and XRD patterns (Figure 3). Figure 2A–D shows hierarchical mesostructures after growth for 10, 20, 30, and 40 min. After the initial 10 min, the macroscopic seed sites (size $< 0.5 \mu\text{m}$) had just begun to form with no recognizable shape. In the XRD (Figure 3A), the appearance of a small hump between 2 and 3° suggests that, at this stage, the nanoparticles have started to self-assemble, exhibiting short range order. After 20 min, the seeds begin to grow into a triangle shape with size between 0.5 and $1 \mu\text{m}$. On the XRD patterns, two peaks are observed at low angle corresponding to cubic symmetry. The first sharp peak is attributed to the (111) reflection, and the second broad hump can be assigned to (220) and/or (311). Between 30 and 40 min, hexagon-shaped subunits with a size of $7 \mu\text{m}$ are developed. They are rather uniform in shape and size. Some of them have merged into hierarchical structures. XRD shows that the fcc mesophase began to form as evidenced by the emergence of (311) and (222) peaks. After 60 min, the hierarchical mesostructures have completely developed, each of which consists of three to five uniformly merged subunits. The XRD (Figure 3A, curve e)

(34) Inagaki, S.; Guan, S.; Ohsuna, T.; Terasaki, O. *Nature* **2002**, *416* (6878), 304–307.

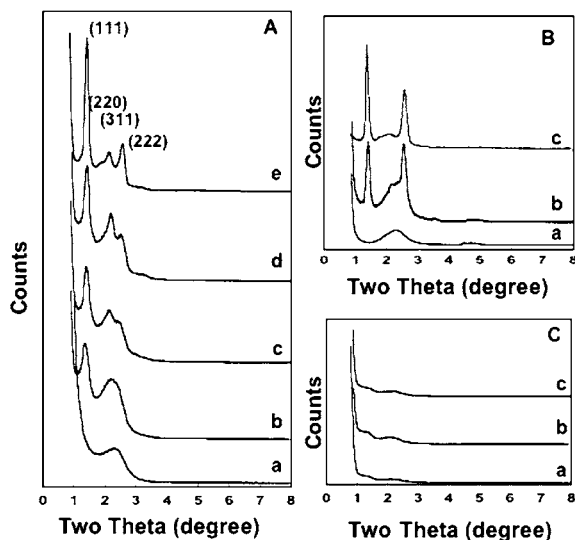


Figure 3. (A) Low angle XRD patterns of hierarchical nanoparticle mesostructure arrays on the glass slide grown (a–e) for 10, 20, 30, 40, and 60 min, respectively. The primary peaks for sample e can be assigned as the (111), (211), (220), and (222) reflections of cubic mesostructure with lattice constant $a = 109.1 \text{ \AA}$. (B) XRD patterns of hierarchical nanoparticle mesostructure arrays on mica grown (a–c) for 10, 30, and 60 min, respectively. (C) XRD patterns of powder samples precipitated in solutions at (a–c) 40, 60, and 120 min, respectively. These patterns show much less order in comparison with those from the hierarchical nanoparticle mesostructures. The samples were prepared using $\sim 2 \text{ nm}$ gold nanoparticles, CTAB surfactant, and sodium hydroxide.

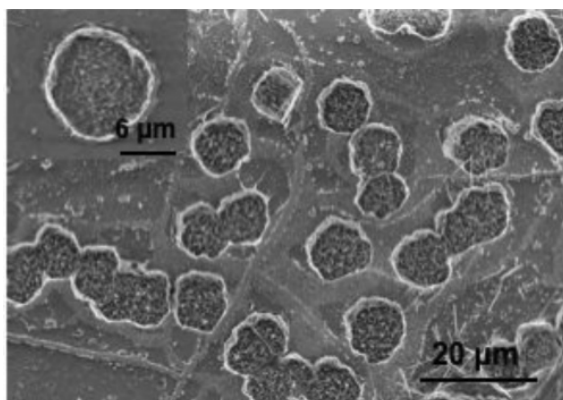


Figure 4. Representative SEM micrograph of hierarchical nanoparticle mesostructure arrays grown on a freshly peeled mica surface using BTEE as the precursor under basic conditions at $100 \text{ }^\circ\text{C}$ for 60 min. Inset: a magnified SEM image showing an individual mesostructure crystal.

suggests that the fcc gold nanoparticle mesostructure has been fully established by the full appearance of (111), (220), (311), and (222) reflections. The enhanced intensity from the XRD reflections of (111) and (222) during the crystal growth course (after 40 min) suggests an orientated growth with (111) planes parallel to the substrate. This is consistent with the shape changes from triangular to hexagonal shape during the growth phase.

Substrate surface properties strongly influence the nucleation and growth of inorganic materials.³⁵ In addition to

amorphous glasses, other substrates such as mica, thermal oxide coated silicon wafer, and photo-curable polymer films have been successfully used to grow hierarchical nanoparticle mesostructures. In a controlled experiment, fresh-peeled mica was used instead of glass, resulting in a distinct crystal shape. Figure 4 shows a typical SEM image of the large nanoparticle mesostructures formed on a mica surface. As with those grown on glass, they are fairly uniform in shape and size ($\sim 12 \text{ }\mu\text{m}$) but possess circular rather than flowerlike topology and have only one single unit instead of several merged subunits. Another remarkable difference is that the orientated mesostructure began to form at 30 min on mica, earlier than on amorphous glass. This could be due to the fact that mica has a crystalline surface with hexagonal patterns that promotes preferential growth along (111) planes. Similar to the case of amorphous glass, the XRD patterns (Figure 3B, curves b and c) show enhanced reflections of the (111) and (222) planes suggesting the (111) planes of nanoparticle cubic mesostructure are parallel to the substrate. It is noteworthy that prior work in self-assembly of silica and surfactants indicated that only a one-dimensional hexagonal mesophase was formed. It was proposed that surfactants form hemi-rod micelles on the mica surface, leading to a one-dimensional surfactant/silica mesophase.³⁶ In the current system, nanoparticle micelles are preformed in a homogeneous aqueous solution. Self-assembly with BTEE starts with “hard sphere” nanoparticle micelle building blocks instead of “soft” pure surfactant micelles or liquid crystals. Thus, the cubic mesophase is preferentially formed.

Following growths longer than 40 min, precipitate was observed in the bottom of the vial. To further explore the formation mechanism, we filtered the growth solution and performed XRD studies on the powders. Figure 3C shows the XRD patterns from the precipitated powders after growth for 40, 60, and 120 min. The irregular patterns suggest much less organized nanoparticle/BTEE arrays. This unambiguously establishes that the hierarchical nanoparticle mesostructures are grown from the solution rather than deposited via precipitation. Any gold nanoparticle agglomeration occurring during growth could be expected to have significant impact on the self-assembly process. A UV–vis spectrometer was used to measure the wavelength of the characteristic surface plasmon resonance, providing a measure of the size dispersity of gold nanoparticle micelles in the solution during the growth process: relative to the original DT capped gold nanoparticles, the gold surface plasmon band exhibited no shift, both for as-prepared solutions and after growth for 40, 60, and 120 min (see Supporting Information, Figure S1). This suggests that the gold nanoparticle micelles remain monodisperse during growth and thus that the formation of the mesophase crystals was initiated from nanoparticle micelle building blocks.

The optical properties of the hierarchical nanoparticle mesostructures have been characterized using UV–visible spectroscopy. Figure 5 shows the UV–vis spectra of the hierarchical gold nanoparticle mesostructures on glass and DT-stabilized gold nanoparticles in chloroform. Both samples

(35) Aizenberg, J.; Black, A. J.; Whitesides, G. M. *Nature* **1999**, *398* (6727), 495.

(36) Yang, H.; Kuperman, A.; Coombs, N.; MamicheAfara, S.; Ozin, G. A. *Nature* **1996**, *379* (6567), 703.

Appendix D: Featured scientific journal publications/cover articles.

3038 *Chem. Mater.*, Vol. 18, No. 13, 2006SELF-ASSEMBLING PROCESS *for* FABRICATING TAILORED THIN FILMS

Wright et al.

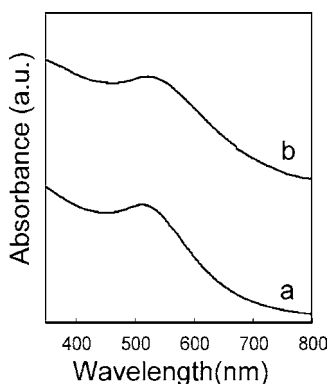


Figure 5. UV-vis spectra of (a) as-prepared DT-capped gold nanoparticles in chloroform and (b) hierarchical nanoparticle mesostructure arrays on the glass slide.

exhibit an absorbance at ~ 519 nm that corresponds to the gold surface plasmon resonance band. By comparison, we observed no difference in the positions and peak widths of the plasmon resonance band from the hierarchical gold nanoparticle mesostructures and the DT-stabilized gold nanoparticles in chloroform, which implies that gold nanoparticles remain monodisperse inside the BTEE matrix without aggregation and that the hydrothermal self-assembly process does not change the optical property of original DT-stabilized nanoparticles. The results suggest the potential applications of these hierarchical nanoparticle mesostructure arrays for SERS-based sensors and integrated optical and electrical platforms.^{2,37} Thermal and mechanical stability is critical for nanoparticle arrays to be applied in practical nanodevices. Heat treatment over time usually broadens the nanoparticle size distribution.³⁸ We expect that the BTEE framework will provide extensive protection from thermally induced particle agglomeration. After crystal growth at 100 °C for up to 3 h, the gold nanoparticles within the hierarchical mesophase crystals remain monodisperse, as shown by TEM (Figure 1C,D). Results from both TEM and UV-vis spectroscopy imply that the inorganic framework provides enhanced thermal stability, preventing gold nanoparticle aggregation or sintering. Additionally, these hierarchical nanoparticle mesophase crystals show seamless self-assembly features without unit cell distortion or shrinking even after heating to 100 °C for several hours, further confirming the mechanical stability.

(37) Chen, J.; Wang, W.; Klemic, J.; Reed, M. A.; Axelrod, B. W.; Kaschak, D. M.; Rawlett, A. M.; Price, D. W.; Dirk, S. M.; Tour, J. M.; Grubisha, D. S.; Bennett, D. W. *Mol. Electron. II* **2002**, 960, 69–99.
 (38) Maye, M. M.; Zheng, W. X.; Leibowitz, F. L.; Ly, N. K.; Zhong, C. J. *Langmuir* **2000**, 16 (2), 490.

Conclusion

We have demonstrated for the first time a new hydrothermal self-assembly process to synthesize hierarchical nanoparticle mesostructures. Results suggest that the formation of such crystals is a nucleation and growth process initiated by self-assembly of nanoparticle micelle building blocks and organo-bridged silane BTEE. The nanoparticles were organized as a cubic mesostructure inside the inorganic framework that allows high-temperature processing. The ease of synthesis of semiconductor and magnetic nanoparticle micelles^{31,32} makes it possible to extend this process to synthesize hierarchically ordered semiconductor or magnetic nanoparticle mesostructures. We expect that by using a variety of optical-, electro-, and magnetic-active organo-bridged silanes as framework, we will be able to synthesize multifunctional mesophase crystals with novel collective physical properties.³⁹ Ultimately, the ordered mesostructure arrays are ideal platforms for fabrication of SERS-based sensors² and charge-transfer-based electronic and optical devices.^{1,4,6,37}

Acknowledgment. This work was partially supported by the U.S. Department of Energy (DOE) Basic Energy Sciences Program, Sandia National Laboratory's Laboratory Directed R&D program, the Air Force Office of Scientific Research, and Center for Integrated Nanotechnologies (CINT). TEM studies were performed in the Department of Earth and Planetary at the University of New Mexico. We acknowledge the use of the SEM facility supported by the NSF EPSCOR and NNIN grants. Sandia is a multiprogram laboratory operated by Sandia Corporation, a Lockheed Martin Company, for the United States Department of Energy's National Nuclear Security Administration under Contract No. DE-AC04-94AL85000.

Supporting Information Available: UV-vis spectra of as-prepared DT-capped gold nanoparticles in chloroform and as-prepared aqueous solution containing gold nanoparticle micelles, and BTEE after addition of NaOH for 1 h and the solutions after growth for 40 and 60 min (PDF). This material is available free of charge via the Internet at <http://pubs.acs.org>.

CM060586+

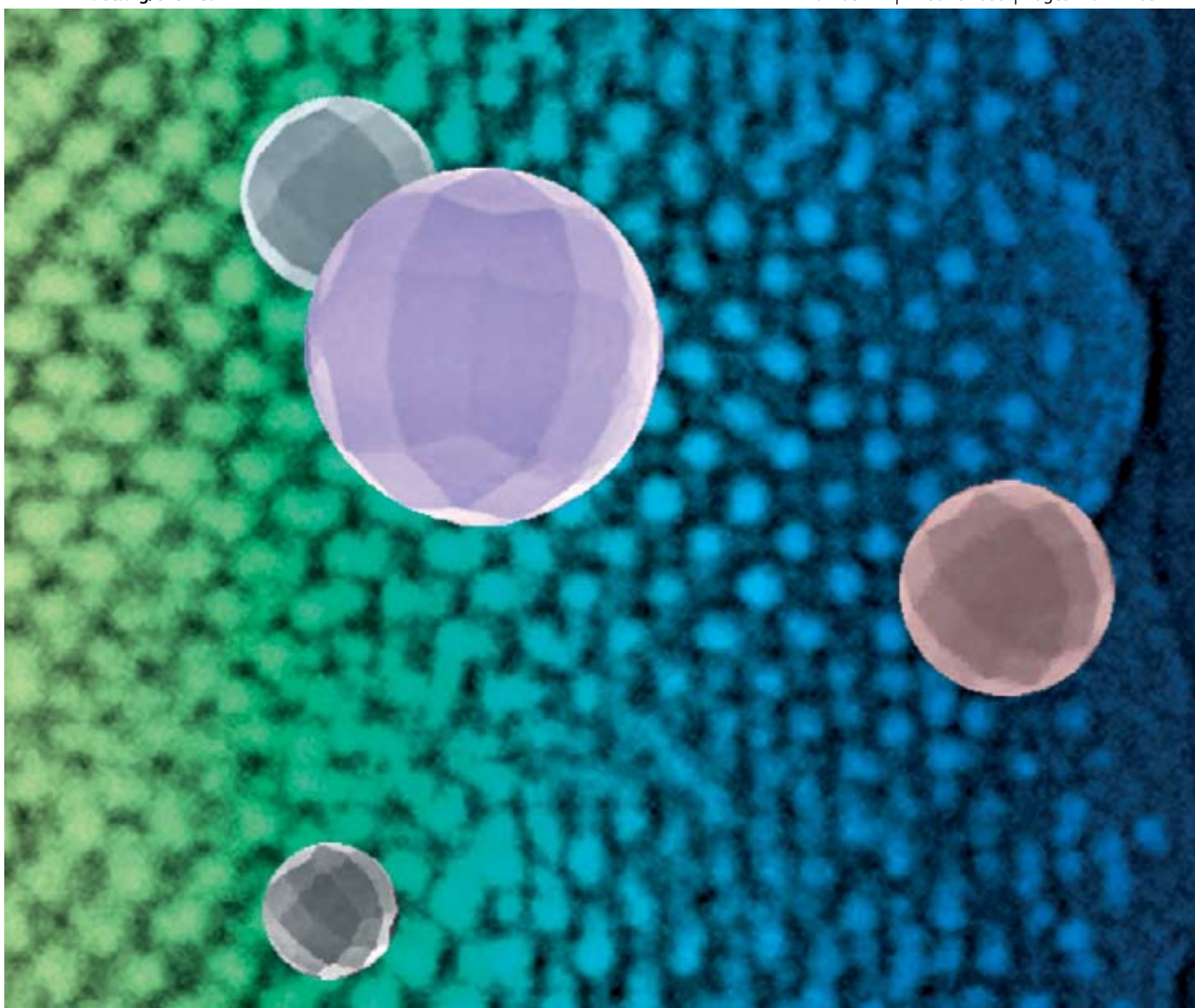
(39) Hatton, B.; Landskron, K.; Whitnall, W.; Perovic, D.; Ozin, G. A. *Acc. Chem. Res.* **2005**, 38 (4), 305.
 (40) Brust, M.; Walker, M.; Bethell, D.; Schiffrin, D. J.; Whyman, R. *Chem. Commun.* **1994**, 7, 801–802.

ChemComm

Chemical Communications

www.rsc.org/chemcomm

Number 22 | 14 June 2006 | Pages 2297–2408



ISSN 1359-7345

RSC Publishing

COMMUNICATION

Hongyou Fan, John Gabaldon, C. Jeffrey Brinker and Ying-Bing Jiang
Ordered nanocrystal/silica particles self-assembled from nanocrystal micelles and silicate

Ordered nanocrystal/silica particles self-assembled from nanocrystal micelles and silicate

Hongyou Fan,^{*ab} John Gabaldon,^b C. Jeffrey Brinker^{ab} and Ying-Bing Jiang^b

Received (in Cambridge, UK) 23rd January 2006, Accepted 14th March 2006

First published as an Advance Article on the web 29th March 2006

DOI: 10.1039/b600923a

Ordered gold nanocrystal/silica particles were synthesized through self-assembly of nanocrystal micelles and silicate. Depending on the use of surfactants, and the kinetic conditions of silica hydrolysis and condensation, well-shaped and irregularly-shaped silica particles were formed, inside which the nanocrystals self-organized in a face-centered cubic mesostructure.

The self-assembly and formation of ordered nanocrystal (NC) arrays have recently received extensive attention due to new physical properties resulting from the coupling of adjacent NCs within the ordered arrays.^{1–8} In general, alkane chain-capped monodisperse NCs were mostly used. Consequently, ordered superlattice arrays were formed by the balanced forces of interparticle attraction and steric interaction due to alkane chain interdigitation. Mesoporous silicas have been used as templates to create hybrid silica materials through direct infiltration of either metal or semiconductor nanoparticles or precursor solutions, followed by chemical reactions (*e.g.*, reduction, *etc.*).^{9–13} In general, the resulting hybrid materials maintained the morphologies of the original template materials, such as film, powder, *etc.* Recently, we have developed a new method for the synthesis of ordered NC/silica arrays.^{3,14,15} In this method, water soluble NC micelles are synthesized through the encapsulation of alkane chain-capped monodisperse NCs within the core of surfactant or block copolymer micelles.^{3,14–17} The self-assembly of NC micelles with metal oxide precursors such as tetraethyl orthosilicate (TEOS) in a controlled homogeneous sol-gel process leads to ordered and uniform NC/silica thin films.^{3,15} The ordered films exhibit a face-centered cubic (fcc) mesostructure. In this communication, we report a heterogeneous self-assembly process to synthesize ordered NC/silica particles, using NC micelles as building blocks to self-assemble with silicate in a controlled low temperature sol-gel process. Depending on the kinetic conditions of silica condensation and the surfactants used to synthesize the NC micelles, both well-shaped and irregularly-shaped silica particles are formed, inside which the NCs self-organize as a fcc mesostructure.

Gold NC micelles were synthesized using our previously developed surfactant encapsulation techniques *via* an interfacially-driven microemulsion process.^{3,14,16,17} 1-Dodecanethiol (DT)-stabilized gold NCs were prepared using the method of Brust *et al.*¹⁸ The NC size distribution was narrowed (<7%) by a

heat treatment and a size selective separation process, according to our previous work.^{14,16} Based on the surfactant encapsulation techniques, the gold NC micelles were synthesized using cetyltrimethyl ammonium bromide (CTAB) and cetyltriethyl ammonium bromide (CTEAB). The extensive van der Waals interactions between the surfactant chains and DT chains leads to an interdigitated “bilayer” structure, stabilizing hydrophobic gold NCs in aqueous solution.^{16,19–21} The NC micelles were stable over a wide pH range, from acidic to basic conditions, allowing facile control of the silica hydrolysis and condensation. In a typical synthesis, acid (HCl) was added to an aqueous solution containing monodispersed gold NC micelle building blocks, followed by the addition of TEOS under vigorous stirring. After 10 minutes of stirring at room temperature, the growth of well-shaped gold NC silica arrays was conducted at 0 °C for 4 days. The powder was collected using a filter and dried in a vacuum furnace at 50 °C overnight. X-Ray diffraction (XRD), scanning electron microscopy (SEM) and transmission electron microscopy (TEM) studies were performed on the samples.

From the SEM images, we observed two distinct particle morphologies. As Fig. 1 shows, the particles prepared using CTEAB-encapsulated NC micelles exhibit a well-defined external surface morphology; the particle size ranging from 3–10 μm. The XRD pattern in Fig. 2D shows three reflections in the low angle region. The primary peaks can be indexed as (111), (221) and (311), based on a fcc mesostructure; the average measured unit cell $a = 10.8$ nm. The TEM images in Fig. 2A reveal that the gold NCs are organized in an orderly manner inside each particle. The measured unit cell from the [100] orientation (Fig. 2B), a , is 10.6 nm, which is close to that obtained from the XRD results. Under identical experimental conditions, particles with irregular surface morphology were formed when using NC micelles prepared by CTAB, with a smaller surfactant head group than that of CTEAB. Fig. 1B shows the SEM image of particles resulting from the synthesis using CTAB-encapsulated gold NC

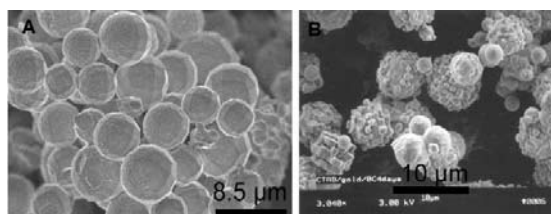


Fig. 1 SEM images of ordered NC/silica particles. A: Particles prepared using CTEAB-encapsulated NC micelles. B: Particles prepared using CTAB-encapsulated NC micelles.

^aChemical Synthesis and Nanomaterials Department, Sandia National Laboratories, Albuquerque, New Mexico 87106, USA.

E-mail: hfan@sandia.gov; Fax: 505-272-7336; Tel: 505-272-7128

^bThe University of New Mexico/NSF Center for Micro-Engineered Materials, Department of Chemical and Nuclear Engineering, Albuquerque, New Mexico 87131, USA

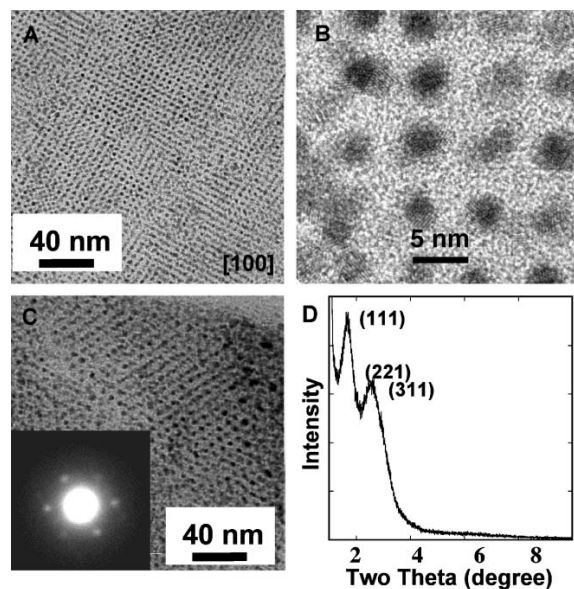


Fig. 2 Representative TEM images and XRD pattern of ordered NC/silica particles. A: [100] orientation of the TEM image of well-shaped and faceted particles in Fig. 1A. B: High resolution TEM of image A. C: TEM image of the irregular particles in Fig. 1B. The inset shows the electron diffraction pattern of image C. D: The XRD pattern of the well-shaped particles in Fig. 1A.

micelles. Most of the particles are composed of many smaller sub-unit particles, with sizes of 1–2 μm and a cubic shape. Despite their irregular topology, the TEM image (Fig. 2C) and electron diffraction pattern (Fig. 2C, inset) indicate that the gold NCs are still organized in an ordered and 3-dimensional fashion inside the particles.

Initial experiments suggest that the formation of faceted gold NC/silica particles is similar to the cooperative self-assembly process to synthesize mesoporous materials.^{22–24} The whole NC micelle behaves as a functional building block having a hydrophilic interface with quaternary ammonium surfactant head groups. These provide sites for further self-assembly with silica to form an ordered mesostructure. According to previous work,^{4,25–27} the NC size distribution is key to achieving highly ordered and faceted superlattice arrays and solids. In our case, after synthesis using the method reported by Brust *et al.*,¹⁸ the initial gold NC size distribution was broad. Subsequent heat treatment at 140 $^{\circ}\text{C}$ for 30 minutes extensively narrowed this distribution.^{28,29} During heat treatment, Oswald ripening occurred, reorganizing the NC sizes and resulting in much more uniform size distribution.^{28,29} In addition, size selective precipitation was carried out using the solvents toluene and ethanol, which made the size distribution less than 7% (size deviation). Encapsulation of such gold NCs within surfactant micelles is driven by an interfacial self-assembly process, in which van der Waals interactions between the hydrophobic alkane carbon chains of CTAB or CTEAB and dodecanethiol stabilize the NC micelle structure through alkane chain interdigitation.^{16,19–21} This is a typical physical chemistry process without chemical reactions being involved, and should not affect the NC size and size distribution after encapsulation. TEM studies

suggest the NC micelles maintain the narrow size distribution of the original gold NCs, consistent with our previous observations.^{3,16,17} According to our recent studies,¹⁵ slow silica gelation kinetics is the fundamental requirement for the formation of ordered NC/silica arrays. Fast silica gelation kinetics lead to an irregular morphology. Under acidic conditions (pH range 1.0–2.0), TEOS first hydrolyses and then forms silica oligomers.³⁰ A low pH and low temperature (0 $^{\circ}\text{C}$) ensured a slow silicate condensation and gelation, which is favorable for the formation of ordered NC/silica arrays. In addition, the balanced hydrogen bonding and charge interactions between the quaternary ammonium groups, silica species and water drive the condensation preferentially at the NC–micelle interface.^{22–24,31} Using a long reaction time (4 days), the slow self-assembly process leads to a well-shaped morphology. Our results suggest that the size of the surfactant head group also plays a critical role in controlling the particle morphology. Although the formation mechanism is not yet clear, we hypothesize that the bigger ethyl head groups of CTEAB take up more of the space surrounding the micelles and block direct and strong interactions between charged silicate species and the quaternary ammonium groups. The weak charge interactions between the silicate species and the quaternary ammonium groups result in a slow assembly, and the formation of a well-organized external topology. However, the smaller methyl groups leave more space for silicate species and result in a stronger interaction with the quaternary ammonium groups, resulting in faster assembly and formation of irregular shapes. This has been observed in other self-assembly systems to synthesize mesostructured silica with a well-defined external morphology.^{32–36}

Currently, more work is being conducted to gain a deeper understanding of the fundamental factors that underlie morphology control, including variations in pH range, the size and type (ionic or non-ionic) of surfactant head group, temperature and reaction time. By using NC micelles prepared with semiconductor and magnetic NCs,^{16,17} we hope that this method can be extended to synthesize similar well-shaped and faceted nanocomposite particles with ordered semiconductor and magnetic NC arrays inside. We expect that these well-shaped NC/silica particles could bring new optical and catalytic properties.

This work was partially supported by the U. S. Department of Energy (DOE) Basic Energy Sciences Program, Sandia National Laboratory's Laboratory Directed R&D Program and the Center for Integrated Nanotechnologies (CINT). TEM investigations were performed in the Department of Earth and Planetary Sciences at the University of New Mexico. We acknowledge the use of the SEM facility, supported by NSF EPSCOR and NNIN grants. Sandia is a multiprogram laboratory operated by Sandia Corporation, a Lockheed Martin Company, for the DOE under contract DE-AC04-94ALB5000.

Notes and references

- 1 C. T. Black, C. B. Murray, R. L. Sandstrom and S. H. Sun, *Science*, 2000, **290**, 1131–1134.
- 2 C. P. Collier, R. J. Saykally, J. J. Shiang, S. E. Henrichs and J. R. Heath, *Science*, 1997, **277**, 1978–1981.
- 3 H. Y. Fan, K. Yang, D. Boye, T. Sigmon, K. Malloy, H. Xu, G. P. Lopez and C. Brinker, *Science*, 2004, **304**, 567–571.
- 4 C. B. Murray, C. R. Kagan and M. G. Bawendi, *Science*, 1995, **270**, 1335–1338.
- 5 M. P. Pileni, *J. Phys. Chem. B*, 2001, **105**, 3358–3371.

Appendix D: Featured scientific journal publications/cover articles.

SELF-ASSEMBLING PROCESS *for*
FABRICATING TAILORED THIN FILMS

- 6 C. A. Stafford and S. DasSarma, *Appl. Phys. Lett.*, 1994, **72**, 3590–3593.
- 7 H. Zeng, J. Li, J. P. Liu, Z. L. Wang and S. H. Sun, *Nature*, 2002, **420**, 395–398.
- 8 K. Yang, H. Y. Fan, K. J. Malloy, C. J. Brinker and T. W. Sigmon, *Thin Solid Films*, 2005, **491**, 38–42.
- 9 Y. Guari, C. Theiuleux, A. Mehdi, C. Reye, R. J. P. Corriu, S. Gomez-Gallardo, K. Philippot and B. Chaudret, *Chem. Mater.*, 2003, **15**, 2017–2024.
- 10 Y. Guari, C. Theiuleux, A. Mehdi, C. Reye, R. J. P. Corriu, S. Gomez-Gallardo, K. Philippot, B. Chaudret and R. Dutartre, *Chem. Commun.*, 2001, **15**, 1374–1375.
- 11 A. Fukuoka, H. Araki, J. Kimura, Y. Sakamoto, T. Higuchi, N. Sugimoto, S. Inagaki and M. Ichikawa, *J. Mater. Chem.*, 2004, **14**, 752–756.
- 12 A. T. Cho, J. M. Shieh, J. Shieh, Y. F. Lai, B. T. Dai, F. M. Pan, H. C. Kuo, Y. C. Lin, K. J. Chao and P. H. Liu, *Electrochem. Solid-State Lett.*, 2005, **8**, G143.
- 13 F. J. Brieler, M. Froba, L. M. Chen, P. J. Klar, W. Heimbrot, H. A. K. von Nidda and A. Loidl, *Chem.–Eur. J.*, 2002, **8**, 185.
- 14 H. Y. Fan, Z. Chen, C. Brinker, J. Clawson and T. Alam, *J. Am. Chem. Soc.*, 2005, **127**, 13746–13747.
- 15 H. Y. Fan, A. Wright, J. Gabaldon, A. Rodriguez, C. J. Brinker and Y. Jiang, *Adv. Func. Mater.*, 2006, DOI: 10.1002/adfm.200500603.
- 16 H. Y. Fan, E. Leve, J. Gabaldon, A. Wright, R. Haddad and C. Brinker, *Adv. Mater.*, 2005, **17**, 2587–2590.
- 17 H. Y. Fan, E. W. Leve, C. Scullin, J. Gabaldon, D. Tallant, S. Bunge, T. Boyle, M. C. Wilson and C. J. Brinker, *Nano Lett.*, 2005, **5**, 645–648.
- 18 M. Brust, M. Walker, D. Bethell, D. J. Schiffrin and R. Whyman, *J. Chem. Soc., Chem. Commun.*, 1994, **7**, 801–802.
- 19 B. Nikoobakht and M. A. El-Sayed, *Langmuir*, 2001, **17**, 6368–6374.
- 20 T. Pellegrino, L. Manna, S. Kudara, T. Liedl, D. Koktysh, A. L. Rogach, S. Keller, J. Radler, G. Natile and W. J. Parak, *Nano Lett.*, 2004, **4**, 703–707.
- 21 L. F. Shen, P. E. Laibinis and T. A. Hatton, *Langmuir*, 1999, **15**, 447–453.
- 22 J. S. Beck, J. C. Vartuli, W. J. Roth, M. E. Leonowicz, C. T. Kresge, K. D. Schmitt, C. T. W. Chu, D. H. Olson, E. W. Sheppard, S. B. McCullen, J. B. Higgins and J. L. Schlenker, *J. Am. Chem. Soc.*, 1992, **114**, 10834–10843.
- 23 Q. S. Huo, D. I. Margolese, U. Ciesla, P. Y. Feng, T. E. Gier, P. Sieger, R. Leon, P. M. Petroff, F. Schuth and G. D. Stucky, *Nature*, 1994, **368**, 317–321.
- 24 Q. S. Huo, D. I. Margolese and G. D. Stucky, *Chem. Mater.*, 1996, **8**, 1147–1160.
- 25 D. V. Talapin, E. V. Shevchenko, C. B. Murray, A. Kornowski, S. Forster and H. Weller, *J. Am. Chem. Soc.*, 2004, **126**, 12984–12988.
- 26 D. V. Talapin, E. V. Shevchenko, A. Kornowski, N. Gaponik, M. Haase, A. L. Rogach and H. Weller, *Adv. Mater.*, 2001, **13**, 1868–1871.
- 27 C. Desvieux, C. Amiens, P. Pejes, P. Renaud, M. Respaud, P. Lecante, E. Snoeck and B. Chaudret, *Nat. Mater.*, 2005, **4**, 750–753.
- 28 M. M. Maye, W. X. Zheng, F. L. Leibowitz, N. K. Ly and C. J. Zhong, *Langmuir*, 2000, **16**, 490–497.
- 29 T. Teranishi, S. Hasegawa, T. Shimizu and M. Miyake, *Adv. Mater.*, 2001, **13**, 1699–1701.
- 30 C. J. Brinker and G. W. Scherer, *Sol–Gel Science: The Physics and Chemistry of Sol–Gel Processing*, Academic Press Inc., San Diego, CA, 1990.
- 31 S. N. Che, S. Y. Lim, M. Kaneda, H. Yoshitake, O. Terasaki and T. Tatsumi, *J. Am. Chem. Soc.*, 2002, **124**, 13962–13963.
- 32 Z. D. Zhang, B. Z. Tian, S. D. Shen, J. Fan, B. Tu, Q. Y. Kong, F. S. Xiao, S. L. Qiu and D. Y. Zhao, *Chem. Lett.*, 2002, 584–585.
- 33 S. Guan, S. Inagaki, T. Ohsuna and O. Terasaki, *J. Am. Chem. Soc.*, 2000, **122**, 5660–5661.
- 34 S. Che, Y. Sakamoto, O. Terasaki and T. Tatsumi, *Chem. Lett.*, 2002, 214–215.
- 35 S. Che, Y. Sakamoto, O. Terasaki and T. Tatsumi, *Chem. Mater.*, 2001, **13**, 2237–2239.
- 36 M. C. Chao, D. S. Wang, H. P. Lin and C. Y. Mou, *J. Mater. Chem.*, 2003, **13**, 2853–2854.

**Appendix E. Excerpts of
Cooperative Research and
Development Agreement**

The CRADA reproduced on the following pages incorporates all amendments to this agreement.

STEVENSON-WYDLER (15 USC 3710)
COOPERATIVE RESEARCH AND DEVELOPMENT AGREEMENT
(hereinafter "CRADA") NO. SC99/01573

Lockheed Martin Umbrella

BETWEEN

Sandia Corporation
(a wholly owned subsidiary of Lockheed Martin Corporation)
As Operator of Sandia National Laboratories
under its U.S. Department of Energy Contract
No. DE-AC04-94AL85000
(hereinafter "Sandia")

AND

Lockheed Martin Corporation and Its Affiliates
(hereinafter "Participant")

Lockheed Martin being a corporation of the State of Maryland
having a principal office in Bethesda, Maryland

Sandia and Participant being hereinafter jointly referred to
as the "Parties."

December 1, 2004

ARTICLE I. DEFINITIONS

- A. "Government" means the United States of America and agencies thereof.
- B. "DOE" means the Department of Energy, an agency of the United States of America.
- C. "Contracting Officer" means the DOE employee administering Sandia's DOE Contract.
- D. "Generated Information" means information produced in the performance of this CRADA.
- E. "Proprietary Information" means information which embodies (i) trade secrets or (ii) commercial or financial information which is privileged or confidential under the Freedom of Information Act (5 USC

**Appendix E. Excerpts of
Cooperative Research and
Development Agreement**

ARTICLE II. STATEMENT OF WORK

Appendix A, Statement of Work, identifies technical categories for projects under this CRADA. Cooperative research is undertaken under this CRADA in accordance with Project Task Statements (PTS) describing specific work falling within one or more of the technical categories set forth in Appendix A. Each specific PTS requires approval by DOE. Appendix A, Statement of Work, and the Project Task Statements are hereby incorporated into this CRADA by reference.

**Appendix A
Statement of Work
CRADA No. SC99/01573**

Lockheed Martin Umbrella

December 1, 2004

A. PURPOSE

The purpose of this CRADA is to develop a range of mutually beneficial technologies to enhance the understanding and application of Advanced Sensors, Advanced Power Systems, Synthetic Environments, Data Transmission and Communications, Information Assurance, Knowledge Management, Compact High-performance Electronics, Photonics and Optical Computing, Unmanned Systems, Computational Fluid Dynamics, and Electromagnetic Launch Technology. Each of these topics are critical to national security and could enhance the effectiveness and competitiveness of one of the largest defense industry leaders in the United States.

Background

This CRADA is a continuation of the DOE Defense Program's initiative to promote synergy of efforts between private industry and the DOE National Laboratories.

Early in 1998, Lockheed Martin's corporate technical office took note of the broad interactions between Sandia and the Lockheed Martin companies and began evaluating technology areas of common interest and mechanisms for streamlining the contractual interactions. The combination of these two drivers (the desire for a streamlined process and the identification of mutual technology interest areas) is the basis for developing the Umbrella CRADA. Lockheed Martin has also identified the funding mechanism with their organizations to make this collaboration possible.

This proposed CRADA will strengthen cooperation and integration of future projects of mutual interest.

Intel Corporation
4100 Sara Road
Rio Rancho, NM 87124-1025
(505) 893-7000
www.intel.com



February 14, 2007

Judging Committee, R&D Magazine
Clearwater Drive
Oakbrook, IL 60523

Dear Judging Committee,

Sandia National Lab partnered with Lockheed Martin Corporation to develop a groundbreaking nanotechnology coating process for the deposition of optical and electrical thin films. The process is simple, flexible, and compatible with current semiconductor fabrication process. The ability to adjust material parameters of the film at the particle synthesis, deposition or post deposition stages with low cost and friendly environment provides a powerful new degree of freedom over conventional deposition approaches.

This process has significant impact in several areas that are important to semiconductor manufacturing. First, the ability to deposit thin films at room temperature drastically reduces dopant diffusion and hence junction shortage. This could also considerably trim down the thermal cost in semiconductor manufacturing due to shrinking devices and shallow junctions. Second, the dimensions of the nanoparticles and low viscosity of the coating solution solvent enable filling of high aspect ratio features, which is difficult for conventional thin film deposition process. Third, unlike top-down deposition approaches, this wet-solution based approach can fill voids with no line-of-site access to the surface. This enables the possibility of 3-D interconnects. Finally, the quantum effects of individual nanoparticle and the collective behavior resulting from the coupling from neighboring nanoparticles bring new physical properties that are not achievable from conventional bulk materials. For an example, the charge hopping behavior within the nanoparticle thin films, in which nanoparticle behaves like a "nano-capacitor" that can hold electrons for a finite time ($\times 5$ seconds), establishes a potential breakthrough building block for fabrication of large memory flash drives.

Overall, this technology represents an important advance in the thin film deposition and brings new opportunities for the semiconductor manufacturing. I strongly support for the nomination of this project for the R&D 100 Award.

Dr. Youren Xu
Manager of New Mexico Materials Lab
Intel Corporation
4100 Sara Road, MIS F9-610
Rio Rancho, NM 87124
Tel: 505-893-1471
Email: youren.xu@intel.com

Lockheed Martin Corporation
6801 Rockledge Drive, Bethesda, MD 20817
Telephone 301-897-6537

LOCKHEED MARTIN



Andrew J. Green
Director, Space Systems Technology

January 26, 2007

The Judging Committee, R&D Magazine
2000 Clearwater Drive
Oakbrook, IL 60523

Dr. Earl Stromberg of Lockheed Martin along with Hongyou Fan, Bruce Burckel and Jeffrey Brinker of Sandia National Laboratories have developed a rapid self-assembly process to engineer optical and electrical nanocrystal films.

As the program manager for Lockheed Martin's Shared Vision program with Sandia National Laboratories I am pleased to recommend this team for an R&D 100 award. This joint project has developed technology that combines surfactant self-assembly and conventional sol-gel processing, producing nanocomposite coatings that exhibit unique optical properties. This enables the development of engineered optical coatings with adjustable properties. The multifunctional ambient deposition of optical coatings eliminate the need for long cycle times and expensive Chemical Vapor Deposition (CVD) capital equipment while providing low stress deposits with improved yields.

This technology will greatly improve many of our current and future products. The nanocrystal films will significantly improve the performance of electro optical targeting systems while driving down the costs due to the increase in reliability. Additional applications of this technology within the Lockheed Martin Corporation include airframes, hulls, and advanced coatings for lenses and mirrors.

I believe that this is a very important technology and that this team is deserving of an R&D 100 award. Thank you for your consideration.

Sincerely,

Andrew Green
Director, Space Systems Technology
Lockheed Martin Corporation

Lockheed Martin Corporation
1011 Lockheed Way, Palmdale, CA 93599



5 February 2007

The Judging Committee, R&D Magazine

The Lockheed Martin / Sandia National Laboratories team has developed a solution-based process employing nanotechnology as an alternate for conventional CVD and sputter deposited optical and electrical films. The intent of this effort is to develop this coating technology in order to provide films that possess similar properties to those films that are fabricated with more expensive deposition processes while enabling tailoring of unique functions and properties. In addition, significant applications for industry and the DoD will be identified along with approaches to integrate this technology into our current / future product lines.

This new technology will require less expensive capital equipment and labor thereby reducing overall cost, more direct applicability to production manufacture which will increase producibility. provide the ability to conduct field repairs which will improve supportability / logistics, and the incorporation of new technology solutions not possible with currently available technology.

The resulting tailorable film process and associated applications will have a significant impact on our products (F-16, F-22, F-35, UAVs, etc.).

A handwritten signature in black ink that reads "John M. Stratton".

John M. Stratton
Director, New Business Funds and CRADA Management
Advanced Development Programs
Lockheed Martin Aeronautics Company

Appendix F. Letters of Support

Lockheed Martin Corporation
6801 Rockledge Drive Bethesda, MD 20817
Telephone 301-897-6000



January 26, 2007

To: The Judging Committee,
R&D Magazine

Gentlemen/Madam:

Dr. Earl Stromberg of our Aeronautics Business Area within Lockheed Martin Corporation (LMC) has been working for over two years with Sandia National Laboratory on a joint collaborative R&D project to develop a rapid, self-assembly process to engineer optical and electrical nanocrystal films. Hongyou Fan, Bruce Burckel and Jeffrey Brinker are the technical collaborators from Sandia.

Sandia is a recognized leader in self-assembled, functional nanomaterials as evidenced by their recent high quality work published in *Nature* and *Science*. Our joint program with them has leveraged Sandia's expertise and experience in the fabrication of self-assembled nanocomposite coatings. The chemistries and processing parameters of the coatings were engineered to develop ones with very specific properties tailored to our applications. In addition to unique chemical and physical properties for our systems, we expect improved durability of the coatings, enhanced supportability, and a low cost, scaleable coatings process. Applications of this technology within Lockheed Martin Corporation are many and include advanced coatings for adaptive micro mirrors, airframes, airship hulls, and fighter jet lenses.

We at Lockheed Martin Corporate who have been funding this project have been very pleased with the results to date. This technology looks to solve some very challenging ones for our corporation. It is a very unique and attractive alternative to conventional Chemical Vapor Deposition (CVD) and sputter deposited optical and electrical films with the added benefits of improved logistics, increased producibility and cost reduction.

It is my pleasure to recommend this team for an R&D 100 award.

Sincerely,

A handwritten signature in black ink, appearing to read "Sharon Smith".

Sharon Smith, Ph. D.
Director, Advanced Technology
Lockheed Martin Corporation



Sandia is a multiprogram laboratory operated by Sandia Corporation, a Lockheed Martin Company, for the United States Department of Energy's National Nuclear Security Administration under contract DE-AC04-94AL85000. SAND2007-0962P Design by Creative Arts. (505) 844-6416 SP•110394•02/07

